Western Washington University

Western CEDAR

Summer 2022

Methane emissions in Port Susan Bay: the missing link in carbon accounting

Rachel S. Yonemura
Western Washington University, rachel.yonemura@gmail.com

Methane emissions in Port Susan Bay: the missing link in carbon accounting

By

Rachel S. Yonemura

Accepted in Partial Completion
of the Requirements for the Degree
Master of Science

ADVISORY COMMITTEE

Dr. John Rybczyk, Chair

Dr. Brooke Love

Dr. David Shull

GRADUATE SCHOOL

David L. Patrick, Dean

Master's Thesis

In presenting this thesis in partial fulfillment of the requirements for a master's degree at Western Washington University, I grant to Western Washington University the non-exclusive royalty-free right to archive, reproduce, distribute, and display the thesis in any and all forms, including electronic format, via any digital library mechanisms maintained by WWU.

I represent and warrant this is my original work, and does not infringe or violate any rights of others. I warrant that I have obtained written permissions from the owner of any third party copyrighted material included in these files.

I acknowledge that I retain ownership rights to the copyright of this work, including but not limited to the right to use all or part of this work in future works, such as articles or books.

Library users are granted permission for individual, research, and non-commercial reproduction of this work for educational purposes only. Any further digital posting of this document requires specific permission from the author.

Any copying or publication of this thesis for commercial purposes, or for financial gain, is not allowed without my written permission.

Rachel S. Yonemura

April 14, 2022

Methane emissions in Port Susan Bay: the missing link in carbon accounting

A Thesis
Presented to
The Faculty of
Western Washington University

In Partial Fulfillment
Of the Requirements for the Degree
Master of Science

By

Rachel S. Yonemura

April 2022

ABSTRACT

Coastal wetlands have the ability to sequester large amounts of "blue carbon" in sediments that would otherwise act as a harmful greenhouse gas in the atmosphere. The recently restored marsh in Port Susan Bay, Washington sequesters $231gC \, m^{-2} \, yr^{-1}$ and accretes 2.75cm of sediment per year. While this restored marsh stores nearly twice as much carbon as the nearby natural marsh, it can also emit methane, a potent greenhouse gas that has the potential to outweigh the benefits of carbon storage. It is critical to measure these emissions to determine if this site is a net source or sink of greenhouse gas potentials. The main objective of this study was to measure carbon sequestration and estimate methane emissions to complete carbon accounting in the restored area of Port Susan Bay. To calculate the most recent rate of carbon sequestration at this site, I used surface elevation table (SET) data from 2021 along with site-specific sediment characteristics and a pre-established ^{210}Pb accretion rate correction factor. Direct, static chamber, methane measurements in the field were unsuccessful due to lack of instrument sensitivity and limited access to the lab. Estimates of methane emissions were made using proxies and published values based on environmental data. The emission estimates were then converted to carbon dioxide equivalents using a global warming potential of 25 and multiplied by the carbon fraction. Environmental data were taken alongside the direct methane measurements at four sites in the restoration area. Samples were taken approximately bimonthly during low tide from Fall 2020 through Summer 2021. I measured salinity, sulfate, redox, sediment temperature, pH, and assessed vegetation percent cover, the results of which all suggest negligible emissions. Average redox was well above -200mV year-round, the level at which methane would be produced. Salinity and sulfate (correlation R-value: 0.76) were high at all four sites in the summer months. The high salinity and sulfate suggest low methane emissions, especially in combination with the

redox values. In these conditions, sulfate reduction is more energetically favorable than reduction

to methane and thus suppresses emissions. While salinity and sulfate were low in the Winter

(0ppt and 50ppm respectively), the low sediment temperature (below 5°C) and high redox

conditions were likely not conducive to extensive, methanogenic microbial activity.

Based on the environmental data, the methane emissions from this site would be between

19.37gCH$_4$ m^{-2} yr^{-1} and 16.4 gCH$_4$m^{-2}yr^{-1}. In terms of greenhouse gas equivalents, this would be

between 110.7gC m^{-2} yr^{-1} and 130.75gC m^{-2} yr^{-1}. The most recent estimate of carbon

sequestration is nearly double the estimated emissions at 206.04gC m^{-2} yr^{-1} suggesting that this

restored site is a net sink of greenhouse gas carbon equivalents. The information from this study

will fill an important data gap to determine if this Pacific Northwest coastal wetland is a source

or sink of greenhouse gas carbon equivalents and help inform future restoration decisions.

ACKNOWLEDGEMENTS

TABLE OF CONTENTS

LIST OF TABLES AND FIGURES

Tables

Figures

Figures

begins. See Appendix E for number of electrodes used at each depth during each sampling period.

1. INTRODUCTION

1.1. Blue Carbon

In addition to providing valuable habitat and ecosystem services (Batker et al. 2008), coastal wetlands sequester "blue carbon" and aid in climate change mitigation (Callaway et al. 2012). "Blue carbon" refers to atmospheric carbon stored by coastal wetlands in long-term accumulating sediments. Atmospheric carbon dioxide originates from natural processes and anthropogenic sources, both of which contribute to climate warming. Uptake of this carbon dioxide occurs through photosynthesis in vegetated coastal wetlands and is stored in sediments (CLEAR 2019). Allochthonous carbon may also add to the carbon deposition in these systems. This carbon storage helps reduce the amount of harmful greenhouse gases in the atmosphere while also building resilience to sea level rise. Restoring coastal wetlands to allow for carbon storage has the potential to be funded by carbon credits, only if the benefits of sequestration outweigh the drawbacks of greenhouse gas emissions.

1.2. Carbon Budget Implications

While coastal wetlands are capable of sequestering large amounts of blue carbon (Mcleod et al. 2011), little is known about the greenhouse gas emissions from these systems. Regardless of carbon sequestration rates in some wetlands, an estimate of carbon emissions is needed to determine whether the system is a source or sink of carbon. If the system is a net source of carbon to the atmosphere (i.e. emits more carbon than it stores), it contributes to climate warming.

In the Pacific Northwest, a few recent studies (e.g., Poppe and Rybczyk 2019, Crooks et al. 2014) report carbon stocks and sequestration rates but not greenhouse gas emission rates. Thus, emission rates represent a data gap in the carbon budget of Pacific Northwest wetlands. The goal

of this project is to complete the carbon budget for the restoration area in Port Susan Bay, Washington; a Pacific Northwest coastal wetland. A carbon budget is comprised of carbon sequestration and carbon emission measurements. I calculated the most recent carbon sequestration rates and estimated the carbon dioxide equivalent of methane emissions using proxies and published values to determine if the restored area of Port Susan Bay is a net sink or source of greenhouse gases. Restored coastal wetlands are of particular interest because restoration can reverse the impacts of wetland degradation. When coastal wetlands are degraded or altered, carbon is released back to the atmosphere (NOAA 2022), contributing to climate warming.

This information is crucial for accurately determining if a wetland is a net sink or source of greenhouse gases and assessing the feasibility of carbon offset credits. Carbon offset credits are a viable incentive only when wetlands are net sinks of greenhouse gases (Murray et al. 2011) and may be overestimated if greenhouse gas emissions are not properly quantified. Once the carbon accounting is completed for a coastal wetland, a carbon standard (such as the Verified Carbon Standard) is needed to verify that carbon credits are assigned properly and that an approved methodology (e.g., VCS) was used to quantify the climate benefits of a potential restoration project. A similar methodology for tidal wetland conservation is currently in development. Given that the need for coastal wetland restoration and conservation far exceeds available funding, the demand for these carbon market mechanisms is tremendous.

The work I conducted will be an important step for carbon accounting; I determined the rates at which carbon is emitted from the restoration area of Port Susan Bay. The type of comprehensive site-scale dataset I developed will be applicable to similar estuaries in the Pacific Northwest

region. Additionally, I have the opportunity to build on a substantial existing body of research from the Port Susan Bay estuary.

1.3. Methane Emissions in Coastal Wetlands

The focus of this project was on methane because it has a high global warming potential, up to 36 times that of carbon dioxide over 100 years (EPA 2017). I chose to use a global warming potential of 25 in my calculations because this value is commonly cited in the literature (e.g. Poffenbarger et al. 2011). Even small methane emissions have the potential to offset the climate benefits of carbon sequestration (Keller 2019). Additionally, there is concern that methane emissions will increase due to rising temperatures and water levels associated with climate change (e.g., Christensen et al. 2003, Holm et al. 2016). Freshwater and brackish marshes are of greater concern than polyhaline marshes because the sulfate in saltier habitats inhibits methane production (Poffenbarger et al. 2011), thus mitigating carbon emissions from the sediment.

Bridgham et al. (2013) defines methane emissions as the "…balance between CH_4 production (methanogenesis) and CH_4 oxidation (methanotrophy)". Wetlands emit more methane to the atmosphere than any other natural source. Globally, they emit an estimated 167 Tg CH_4 yr^{-1} compared to 231 Tg CH_4 yr^{-1} for all natural sources (Dean et al. 2018). Increased methane emissions with climate change are troublesome because many ecosystems are likely to undergo alterations that could impact emissions as the climate changes (e.g. Morgan and Siemann 2011). Methane production in wetlands occurs under anoxic conditions facilitated by waterlogging. Waterlogged environments allow for carbon sequestration through inefficient respiration of organic matter due to the lack of oxygen, but consequently enable methane emittance (Dean et al. 2018), by methanogens. Methanogens are microorganisms that produce methane and use carbon dioxide as their electron acceptor (Mitsch and Gosselink 2015). Once produced, methane

3

is released from wetlands through diffusion, ebullition, and plant-mediated transport (Bridgham et al. 2013, Whalen 2005).

1.4. Carbon Measurement Methods in Coastal Wetlands

A complete carbon budget reflects the balance of carbon storage and carbon emissions. To complete the carbon budget for the restoration area of Port Susan Bay, I report the most recent carbon accumulation rate and compare it to the carbon dioxide equivalent of methane emissions from the site using a global warming potential of 25.

The original intention of this project was to directly measure annual methane emissions in the field using the static chamber method along with a suite of ancillary data. This method uses linear regression to calculate methane flux as it builds up in a fixed-volume chamber over time. I designed and constructed three identical static chambers using polyvinyl chloride pipes, plexiglass, and a sleeve-type septa similar to Gunn (2016). The chambers were left on the sediment surface during low tide for 60-90 minutes and headspace samples were taken every 15 minutes. These samples were then run on a gas chromatograph with a flame ionization detector. After several sample runs on the gas chromatograph, we determined that the instrument was not sensitive enough for the Port Susan Bay samples, even when the instrument baseline was accounted for. The analysis and instrumentation setup were also compromised due to limited laboratory access during Covid-19.

According to the Intergovernmental Panel on Climate Change (IPCC), ancillary data can be used as proxies to provide estimates of methane emissions (VCS 2015). I measured salinity, sediment temperature, sulfate, redox, pH, vegetation composition, and aboveground biomass alongside the chamber measurements. These factors were used as proxies to assess methane emissions in the

restored area of Port Susan Bay. Default factors and published values complemented the proxy data to provide a more comprehensive estimate.

Long-term carbon accretion is commonly reported using ^{210}Pb dating. This method determines carbon accumulation rate as a function of ^{210}Pb decay and sediment carbon density. Poppe and Rybczyk (2021) measured carbon accretion in the Port Susan Bay, Washington at 13 sites throughout the estuary using ^{210}Pb dating. They also measured carbon accumulation using 21 permanent surface elevation tables (SETs). A SET is a monitoring device used to measure relative elevation change over time. To determine carbon accumulation using SET data, the relative elevation change rate is multiplied by carbon density and subsequently corrected using a ^{210}Pb to SET ratio for that specific site. For this project, I calculate the most recent carbon accumulation rates for Port Susan Bay using SET measurements from 2021 to assess carbon storage and compare to carbon loss through methane emissions.

Neubauer (2021) describes a greenhouse gas flux corrected by its respective global warming potential as a "CO_2-equivalent greenhouse gas flux". I will use this term along with," greenhouse gas carbon equivalents" to describe the carbon dioxide equivalent of methane emission estimations. To compare the carbon dioxide estimates to carbon sequestration, I will further multiply that "CO_2-equivalent greenhouse gas flux" by the carbon fraction in carbon dioxide to account for just the carbon. I only account for the carbon originating from methane estimates in this project and do not include estimates for other greenhouse gas emissions such as carbon dioxide, nitrous oxide, or fluorinated gasses.

1.5. Study Site

Port Susan Bay is a recently restored tidal marsh on the northwest coast of Washington State (Figure 1). It is situated in Puget Sound just south of Stanwood, Washington in Snohomish

County; part of the greater Stillaguamish watershed. The Nature Conservancy purchased the land in 2001 and continues to manage it. In 2012, 1.4 miles of dike were breached to incorporate an additional 150 acres, of what used to be farmland, back into the estuary. This allowed for more freshwater mixing from the Stillaguamish River, critical habitat and marsh restoration, and resilience to sea level rise (Fuller 2018). Since the dike has been removed, the site has been accreting about 3.1 centimeters of sediment per year (Poppe and Rybczyk 2019), outpacing current and predicted rates of sea level rise.

The Wetlands Ecology Lab at Western Washington University along with The Nature Conservancy has conducted pre- and post-restoration monitoring throughout Port Susan Bay. This included the establishment of 21 surface elevation tables (SETs) in five zones and a study to quantify carbon stocks and sequestration rates at 13 sites coinciding with the SET locations (Figure 2). The research demonstrated that the tidal marshes across the estuary are sequestering carbon at high rates, particularly within the restored marsh; $230gCm^2y^{-1}$ in restored area and $123gCm^2y^{-1}$ in adjacent natural marshes (Poppe and Rybczyk 2019). Post-restoration monitoring from 2015 revealed that salinity has overall decreased since the dike has been removed, the highest salinities are furthest from the river, and that salinity is highest during the summer (The Nature Conservancy 2015).

Previous research includes vegetation, salinity, and sediment surveys, hydrology monitoring, elevation change monitoring, and recent studies of carbon stocks and sequestration rates.

Four sites were established in the restoration area (Zone 2, Figure 2) specifically for this project (Figure 3). Two sites are in the middle of the restoration area (RM1 and RM2) and the other two are at the southern end near the Stillaguamish River (RS1 and RS2).
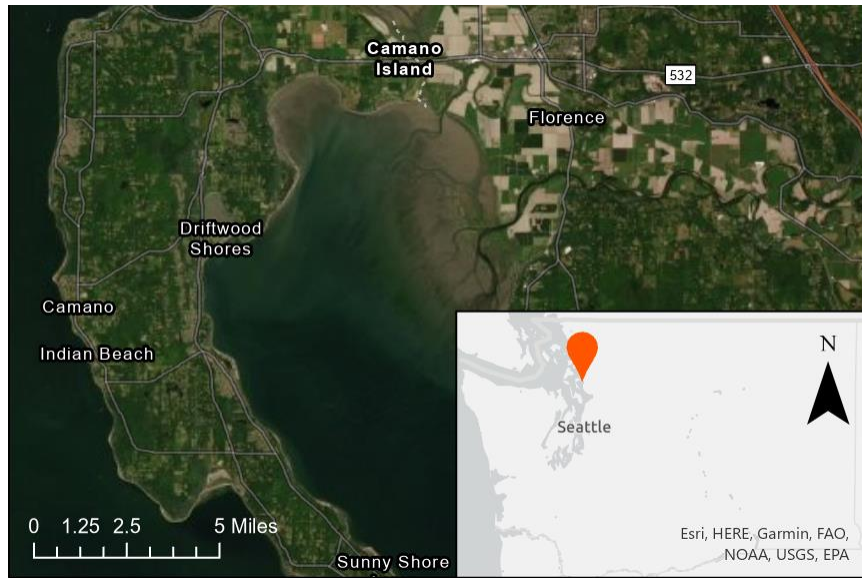
Figure 1. Port Susan Bay, Washington (48.208372, -122.365763).
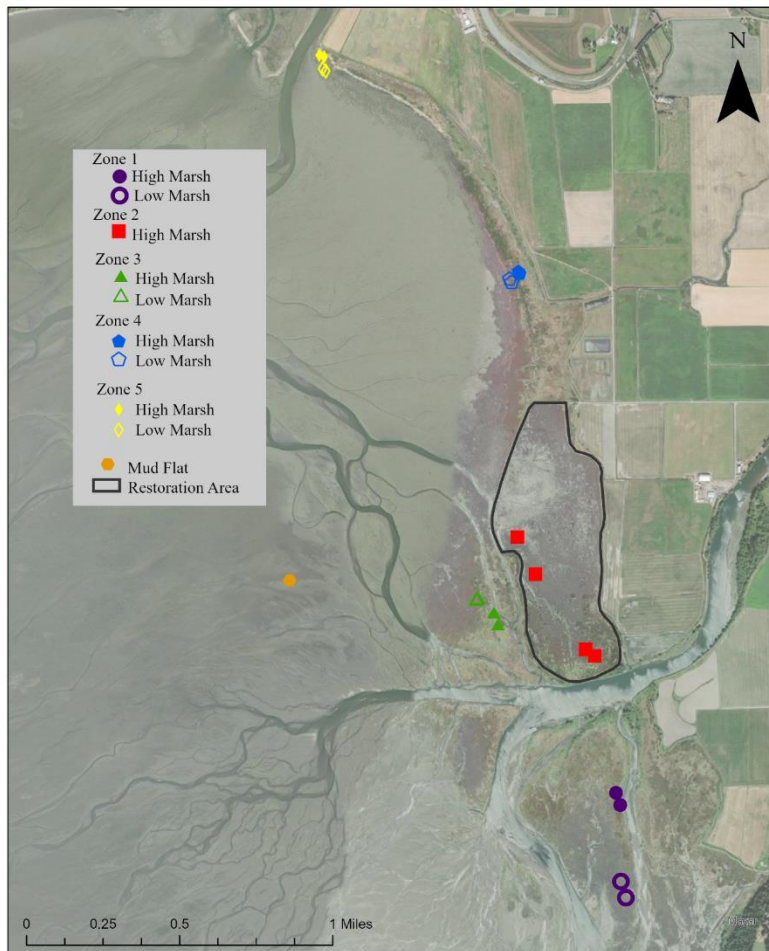
Figure 2. SET and restoration locations in Port Susan Bay, WA. Restoration area outlined in black. Solid points depict high marsh sites and hollow points depict low marsh sites.

1.6. Objectives

The goal of this study was to complete the carbon budget for the restored area in Port Susan Bay, Washington; to assess whether it is a net source or sink of carbon. I used the most recent elevation change rates and carbon density at each SET to calculate carbon accumulation and I used proxies to estimate annual greenhouse gas carbon equivalents of methane emissions. Additionally, I customized a simple, cost-effective field method of measuring methane. The following objectives outline the work presented in chapters 2, 3, 4 and Appendix A:

2. *Estimate methane emissions in restored area of Port Susan Bay, Washington using proxies.*

    a. Measure proxies: salinity, sulfate, redox, sediment temperature, pH, and vegetation composition.

    b. Analyze correlations between variables and similarities between sites.

    c. Use default factors, emission factors, and published values to estimate annual methane emissions in restored area.

3. *Calculate updated carbon accumulation rates.*

    a. Calculate elevation change rate from 2021 relative to initial SET measurements.

    b. Calculate updated rate of carbon accumulation using latest elevation change rate, carbon density, and long-term accretion correction factor.

4. *Determine if the restoration area is a net source or sink of greenhouse gases.*

    a. Calculate carbon budget for restoration area of Port Susan Bay by comparing carbon sequestration and carbon emissions via methane.

Appendix A. *Customize a cost-effective methane measurement method for coastal wetlands.*

    a. Design and build static chambers for field deployment.

    b. Deploy chamber in the field and take headspace measurements.

    c. Analyze samples on gas chromatograph fixed with a flame ionization detector (GC-FID).

2. EMISSION ESTIMATES IN PORT SUSAN BAY

2.1. Introduction

2.1.1. Importance of Methane Emission Measurements

Methane emissions ($gCH_4\, m^{-2}\, yr^{-1}$) from coastal wetlands can outweigh the benefits of carbon sequestration. According to the Verified Carbon Standard (VCS) Methodology for Tidal Wetland and Seagrass Restoration, methane emissions can be estimated using field-collected data, proxies, models, default factors, published values, or Intergovernmental Panel on Climate Change (IPCC) emission factors (VCS, 2015). A proxy, as defined by the VCS Program Definition, is "a parameter that is monitored or measured to determine the value of a strongly correlated parameter that is not monitored or measured" (VCS, 2021). The covariates listed for use as proxies by the VCS that I used in this project include: salinity, temperature, soil organic carbon, sulfate concentrations (VCS, 2014), as well as redox. I also measured pH, vegetation composition, and biomass as ancillary variables. These proxies provide an estimate of methane emissions which are otherwise difficult to measure in the field due to equipment, time, and monetary constraints. While portable instantaneous samplers cost thousands of dollars (e.g. Fourier-transform infrared), lower-cost chambers require longer deployment times in the field and subsequent lab analysis (e.g. Derby et al. 2021).

Little is known about methane emissions in Port Susan Bay, WA. This information is crucial to accurately determine if this coastal wetland is a net source or sink of greenhouse gases. Further, measuring methane emissions at this site will help determine the feasibility of selling carbon offset credits. Purchasing a carbon offset credit permits the emission of one ton of carbon dioxide or other greenhouse gas equivalent. These credits are a viable incentive only when wetlands are net sinks of greenhouse gases (Murray et al. 2011) and may be overestimated if greenhouse gas

emissions are not properly accounted for. As mentioned above, I measured several proxies for methane emissions in the restored area of Port Susan Bay, WA with the goal being to estimate greenhouse gas carbon equivalents of methane emissions at this site.

2.1.2. How Proxy Factors Influence Methane Emissions

2.1.2.1. Salinity

Salinity in estuaries is spatially and temporally variable and is influenced by tidal cycles and freshwater inputs (NOAA 2017). Salinity ranges from 6ppt to 20ppt in Port Susan Bay, WA marshes (Poppe and Rybczyk, 2021). Methane emissions are generally negatively correlated with the salinity gradient from freshwater to the ocean (e.g. de Angelis et al. 1987). Poffenbarger et al. (2011) suggest that the upper limit of methanogenesis is determined by salinity. Specifically, wetlands with salinities greater than 18ppt have significantly lower methane emissions than wetlands with salinities less than 18ppt (Poffenbarger et al. 2011). This because saltwater typically has more sulfate ions than freshwater allowing sulfate-reducing bacteria to outcompete methanogens (Mitsch and Gosselink 2015).

Salinity is listed as a proxy covariate by the VCS to estimate methane emissions, but it is important to take other factors into consideration.

2.1.2.2. Sulfate

Sulfate is common in coastal wetlands. The average sulfate concentration in seawater is 2,712ppm and 11.2ppm in freshwater (Mitsch and Gosselink 2015). Sulfate from seawater is important for methane emissions because methanogens can be competitively suppressed by alternate terminal electron acceptor processes such as sulfate reduction (Bridgham et al. 2013). Sulfate is a major electron acceptor following oxygen, nitrate, iron, and manganese, all of which yield more energy during respiration than carbon dioxide reduction (i.e. methane production).

Tidal inundation can replenish sulfate concentrations, making the environment more favorable

for sulfate reduction. Typically, salinity can be used as an indicator for sulfate concentration, but

there can be localized areas of sulfate depletion due to sulfate reduction (Poffenbarger et al.

2011). Assuming that sulfate is in constant proportion relative to salinity is not justified in these

conditions and is another reason why it is crucial to measure sulfate concentrations alongside

salinity.

2.1.2.3. Redox

Mitsch and Gosselink (2015) define redox potential as "…a measure of the electron pressure (or

availability) in a solution" and is used to measure relative reduction in soils. Sulfate acts as a

terminal electron acceptor following oxygen, nitrate, manganese oxide, and iron oxide as the

redox potential decreases (Mitsch and Gosselink 2015). This hierarchy is based on energy yield

where the reduction of oxygen>nitrate>manganese (IV)>iron(III)>sulfate>carbon dioxide.

Oxygen reduction yields nearly 100 times more energy than carbon dioxide reduction. The redox

potential for transformation range for oxygen is between 400mV and 700mV whereas sulfate

ranges from -100mV to -200mV and carbon dioxide is below -200mV (Table 1, Mitsch and

Gosselink 2015). Redox measurements indicate which electron acceptor is being reduced in the

sediment and, consequently, what is being emitted and transformed in the soil in vertical

succession.

Table 1. Redox Potentials summarized from Mitsch and Gosselink 2015

Oxidized Form	Reduced Form	Redox Potential (mV) for transformation
Oxygen	Carbon dioxide, water	400-600
Nitrate	Nitric oxide, nitrous oxide, dinitrogen	250
Manganic	Manganous	225
Ferric	Ferrous	100 to -100
Sulfate	**Sulfide**	-100 to -200
Carbon Dioxide	**Methane**	Below -200

2.1.2.4. Temperature

Temperature influences methane emissions by controlling microbial activity. Methane emissions are positively correlated with seasonal temperature fluctuations; emissions are typically highest during the summer months (e.g. Harley et al. 2015 and Hu et al. 2016). Using random forest models, Schultz (2019) found soil and air temperature important for explaining methane emissions in Tillamook Bay and Coos Bay, Oregon.

2.1.2.5. pH

Slight deviations in pH can impact methane emissions. Wang et al. (1993) suggest that slight decreases from neutral pH can decrease methane emissions while increases can enhance emissions. Schultz (2019) found pH to be a more important indicator of methane emissions than salinity after water table and temperature in Tillamook Bay, Oregon. There is uncertainty about how pH interacts with different factors influencing methanogenesis other than oxidation likely decreases pH and methanogenesis and reduction increases pH and methanogenesis.

2.1.2.6. Vegetation Composition

Derby et al. (2021) suggested that plant composition is a promising proxy for methane emissions. The ability of plants to oxidize the rhizosphere can influence the balance of electron acceptors in the sediment (Neubauer et al. 2005), and ultimately reduce the rate of methanogenesis. Plants can also facilitate the movement of methane produced in the sediments via transport through arenchymous tissue, termed plant-mediated transport (Whalen 2005). This methane can either be emitted to the atmosphere or oxidized before it reaches the atmosphere (Laanbroek 2009). There are many factors that influence how plant species interact with sediment biogeochemistry, but some studies suggest that certain species are more conducive to emitting methane than others. Of seven graminoid species studied, Kao-Kniffin et al. (2010) found the forbs *Phalaris arundinacea*

and *Typha angustifolia* to have the lowest methane emissions whereas *Carex stricta* and *Scirpus atrovirens* had the highest (with the two forb species not producing any). Bhullar et al. (2013) also found graminoid species to have higher emissions than forbs.

2.1.2.7. Biomass

There is a tradeoff between methane oxidation and methanogenesis facilitation with an increase in biomass. For example, Kao-Kniffin et al. (2010) found low methane emissions by *Phalaris arundinacea* and *Typha angustifolia* despite high productivity and appropriate vascular structure. Kao-Kniffin et al. (2010) hypothesized that this occurred because of the plants ability to oxidize the sediments. This relationship is not consistent among all species. Similarly, Bhullar et al. (2013) found a negative relationship between biomass and methane emissions despite a positive relationship between biomass and "percent chimney effect", meaning that plants with a larger root volume can transport more methane than plants with smaller root volumes.

2.1.2.8. Sediment Organic Matter

Sediment organic matter is an essential, and natural, component of nutrient cycling in estuarine systems (NOAA 2017). Several studies have found methane production to be correlated with primary production and stimulated by photosynthate from root exudates (Bridgham et al. 2013). Methanogens use components of organic matter as substrates for methanogenesis. Thus, organic matter quality can be an indicator for anaerobic degradation (Dean et al. 2018). Organic matter can vary spatially within any given system and can be influenced by the water regime (Mitsch and Gosselink 2015). For example, higher dissolved methane concentrations have been found in areas of high dissolved organic carbon (Looman et al. 2019). Looman et al. (2019) observed that an unaltered system had higher dissolved organic carbon than in an urban-agriculture system.

2.2. Methods

I began fieldwork in August 2020 and completed it in September 2021. I took field

measurements during low tides every month during the summer and once in the fall and winter.

Four sites (southern sites: RS1, RS2, and middle sites: RM1, and RM2) were established in the

restoration area at the beginning of the project (Figure 3). Each site is within approximately 25 to

75 meters east of the four SETs to pair with preexisting data and limit sediment disturbance near

the SET equipment. Subsequent laboratory analyses took place within 30 days of each field

outing.

I revisited the same sites each month when possible. There were a couple months when the exact

sites were either covered with wrack or unrecognizable. In that case, I took measurements as

close to the same spot as possible. Approximate geographic coordinates of each site center are

listed in Table 2.

Table 2. Sampling site locations in Port Susan Bay, Washington

Site	Latitude	Longitude
RS1	48.198487	-122.364253
RS2	48.198765	-122.364924
RM1	48.202357	-122.368242
RM2	48.20408	-122.369151
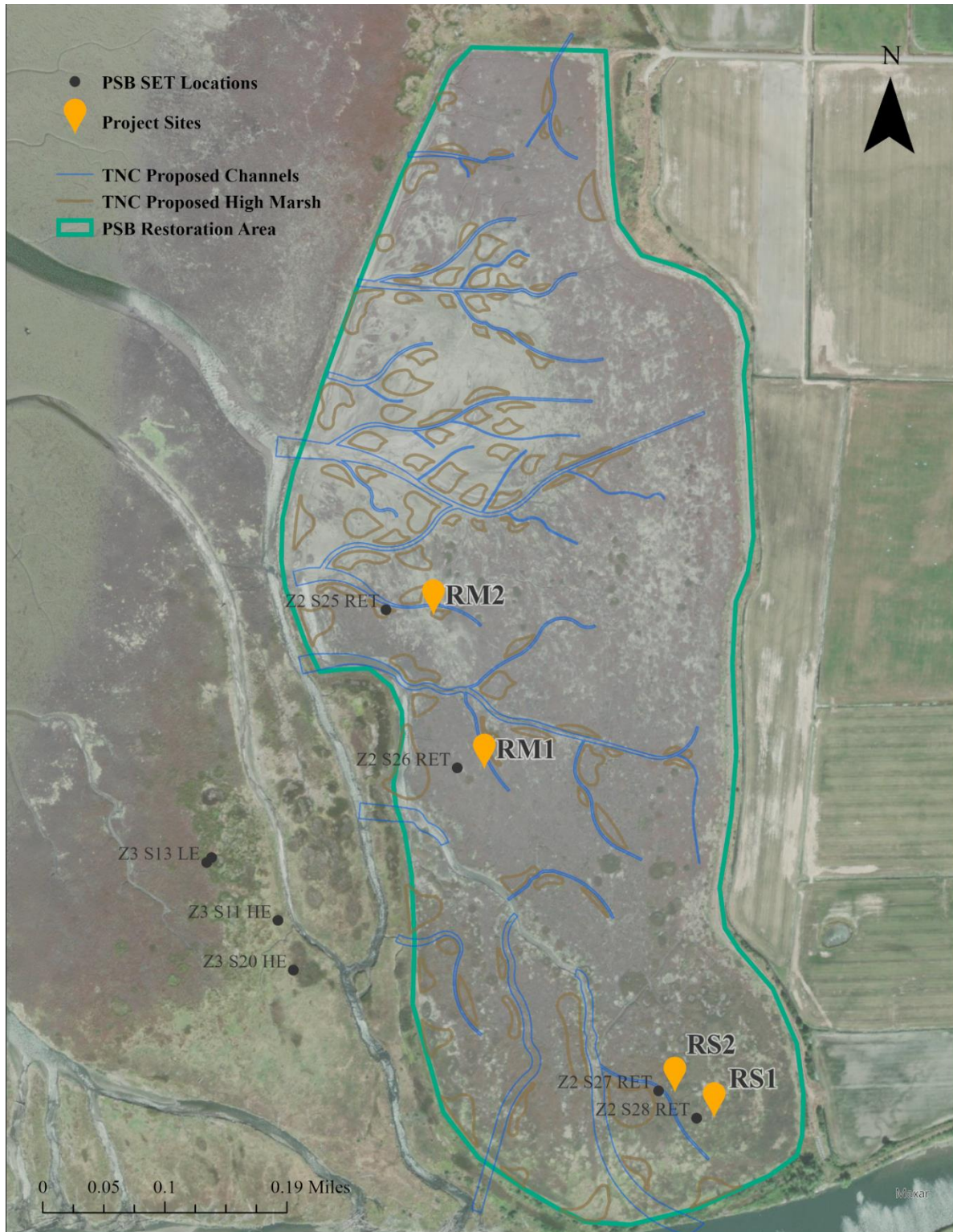
Figure 3. Map of restoration area at Port Susan Bay, WA outlined in green. Orange markers denote sites RM1, RM2, RS1, and RS2 (coordinates listed in Table 2). Black dots represent pre-existing SET locations. The Stillaguamish River runs just south of the restoration site and the dike creates the eastern border.

2.2.1. Field Methods

Each site (RS1, RS2, RM1, and RM2) was split into three sub-sites so that I could get consistent, triplicate measurements (Figure 4). "Rep 1" was roughly five to ten meters north of the center, "rep 2" to the west, and "rep 3" to the south. Some sites were more difficult to establish than others creating a slightly different arrangement. Redox and general observations were taken at the center and all other measurements were taken as triplicates at each replicate site.
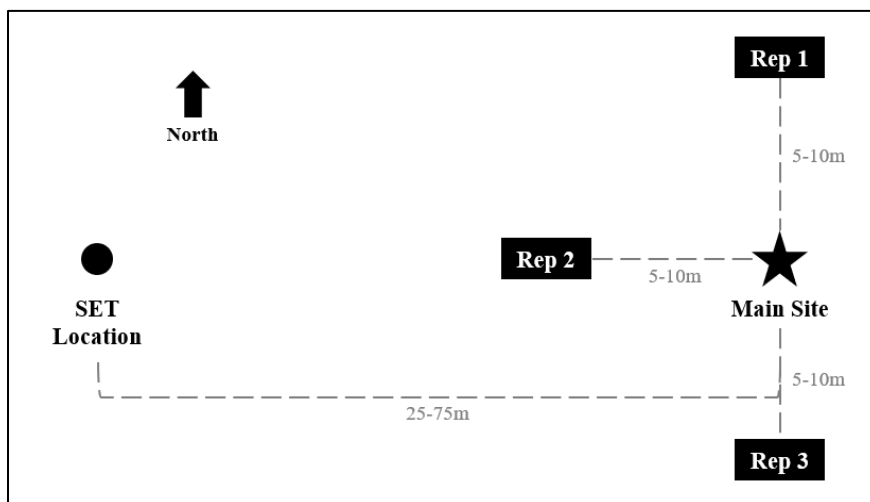
Figure 4. Sampling layout at each site relative to SET location. Main site represents RM1, RM2, RS1, and RS2 and "Rep 1", "Rep 2", and "Rep 3" denote replicate sites.

2.2.1.1. Porewater Measurements: Salinity, Sulfate, pH, and hydrogen sulfide

Salinity, sulfate, pH, and hydrogen sulfide were measured from pore water at each triplicate site. I dug a 15-centimeter-deep pit when we arrived at site and let it fill with water (Figure 5a). The water intended for the determination of salinity and sulfate was filtered through a 0.22µm filter using a 30-ml syringe (Figure 5b) whereas the water used for pH and hydrogen sulfide was not. The environmental conditions (e.g. sediment type, tides) and time in the field were not conducive to using a sipper to minimize pore water disturbance. A sipper is used for minimally-destructive pore-water sampling. It is comprised of glass capillary tubing and a serum stopper (Howels et al.

16

1985). Water is withdrawn out of the serum stopper with a syringe. Howes et al. (1985) found

that salinity and sulfate were not impacted by pore-water sampling technique; whether

destructive or not.

a.   b.
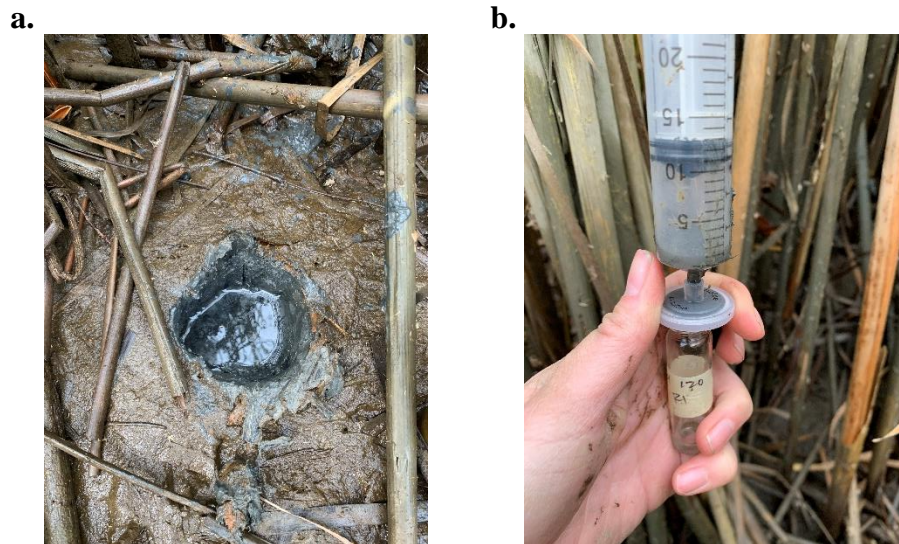
Figure 5. Porewater sampling pit (a) and sampling syringe with filter (b).

2.2.1.1.1.   Salinity

I took one salinity reading at each replicate site using a Vee Gee refractometer (model

A366ATC). A few drops of filtered pore water were placed on the prism, the cover plate was

closed, and salinity was read in parts per thousand by pointing the refractometer toward the sun

(Figure 6a&b). A flashlight was used as the light source during night measurements.

Refractometers measure the concentration of sodium and chloride ions by comparing the

refractive index to the refraction angle of the solution (Cole Parmer Refractometers).

Figure 6. Refractometer reading (a) and refractometer sample preparation (b).

2.2.1.1.2. Sulfate

Five to ten milliliters of filtered pore water were collected at each replicate site and placed in small glass vials for sulfate analysis. I kept the water samples on ice until returning to the lab where they were stored in the freezer, consistent with EPA methods for ion chromatography (Eurofins, 2016). All the water samples were analyzed on the high-performance liquid chromatography (HPLC) instrument for sulfate concentrations within 30 days of collection.

2.2.1.1.3. pH

I measured pH using a hand-held Oakton PhTestr (35634-10) field probe at each replicate site. I inserted the pH probe directly into the large end of the syringe and waited for it to stabilize (Figure 7). The pH meter was calibrated at the beginning of each field day using 4, 7, and 10 pH N-Bromosuccinimide buffers.

Figure 7. Hand-held meter reading porewater pH.

2.2.1.1.4. Hydrogen Sulfide

I measured hydrogen sulfide to get a rough idea of free sulfide concentrations in the environment. Sulfide can oxidize to sulfate and thus skew the sulfate measurements if the water samples are not properly stored. I used Industrial Test Systems WaterWorks test strips (0-80ppm) to test for hydrogen sulfide. I dipped the test strip in the unfiltered water at each replicate site and read the concentrations based on a color chart (Figure 8).

Figure 8. Hydrogen sulfide test strip against color chart.

2.2.1.2. Redox

Redox was measured using platinum electrodes (Figure 9). I measured redox at two depths (2.5 and 15 centimeters) at each main site. Before placing the electrodes in the sediment, I carefully made holes using a skewer as to not damage the electrodes. Both ends of the electrodes were cleaned and sanded before measurements to ensure good conductivity. Four to 16 electrodes were left to equilibrate before measuring in millivolts using a volt meter (see Appendix E for equilibration times and number of electrodes per depth). A calomel electrode was connected to the voltage meter as the reference electrode. I added 244 to the final reading to correct for the calomel electrode potential (in millivolts).

Platinum electrodes were calibrated in winter 2021 using quinhydrone and a pH 4 buffer. I considered the few values above 700mV and below -300mV outliers and did not include them in the statistical analyses or plots.

Figure 9. Redox electrodes equilibrating at 2.5cm in the sediment with calomel electrode in the middle. Voltage meter and leads on lower left.

2.2.1.3. Vegetation

I used a one square meter quadrat to estimate percent cover of all dominant plant species at each replicate site (Figure 10a&b). The quadrat was randomly placed approximately one meter away from each chamber.
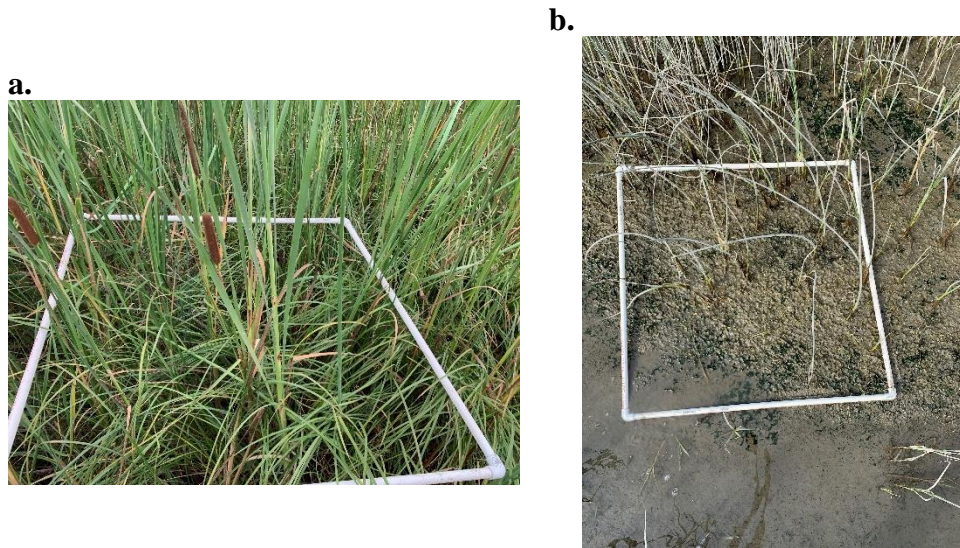
Figure 10. Sample $1m^2$ vegetation plots at RS1 (a) and RM2 (b).

2.2.1.4. Peak Standing Crop

In August 2020 I collected vegetation samples to estimate peak standing crop using clip plots to assess aboveground biomass. I partitioned the one square meter vegetation quadrat into four sections and collected all the aboveground vegetation in the lower right 0.25 square meter portion (Figure 11). I refrigerated the samples for one week before analysis.
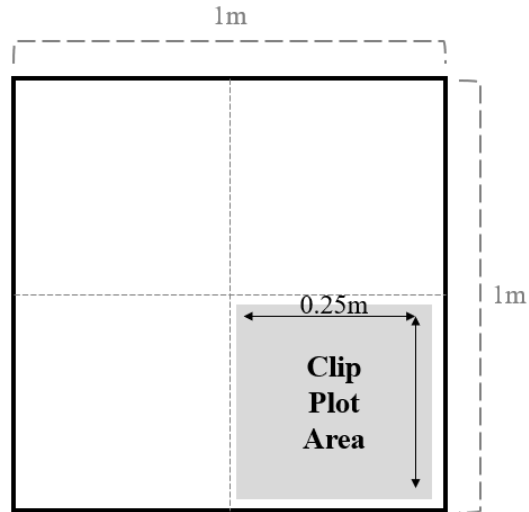
Figure 11. Clip plot layout. Clip plot ($0.25m^2$) was taken in lower right corner of $1m^2$ quadrat.

2.2.1.5. Sediment Temperature

I measured sediment temperature using an electrical metal thermometer three times at each replicate site for a total of nine readings per site. The thermometer was placed 10 centimeters into the sediment and left until stabilized.

2.2.1.6. Environmental Conditions: tide height and weather

I recorded tide height using the Tide Graph Apple application. I used the Kayak Point, Washington (48.135421, -122.368103) station, rightly five miles south of the restoration area, as a conservative estimate of the tide height to plan fieldwork dates. I used the Apple Weather application to record ambient temperature, pressure, and humidity for Stanwood, Washington.

2.2.2. Laboratory Methods

2.2.2.1. Peak Standing Crop

All vegetation samples were stored in the refrigerator to minimize decomposition and analyzed within one week of collection. I separated all samples to isolate only living vegetation. The living vegetation was dried in an oven at 60 degrees Celsius for one week and subsequently

22

weighed. After weighing all the samples, I calculated biomass per square meter by multiplying

the biomass of each 0.25 square meter replicate site by four.

2.2.2.2. Sulfate

Frozen water samples were thawed and filtered a second time using a 0.22µm filter before

analysis (Figure 12a). Sample dilutions and injection volumes varied among samples and dates

based on initial concentrations. Sample dilutions ranged from zero to 1:48 with deionized water

and injection volumes were typically either 5µl or 10µl. The filtered, diluted samples were then

run on the Agilent 1100 high-performance liquid chromatography (HPLC) instrument using a

Thermo Scientific Dionex IonPac AS-22 fast column (Figure 12b). The flow rate was set at

1.5mL/min and the running buffers were 4.5mM Na_2CO_3 and 1.4mM $CaHCO_3$. The sulfate

standards used were 2.5, 5, 10, 15, 20, and 30ppm.

a.   b.
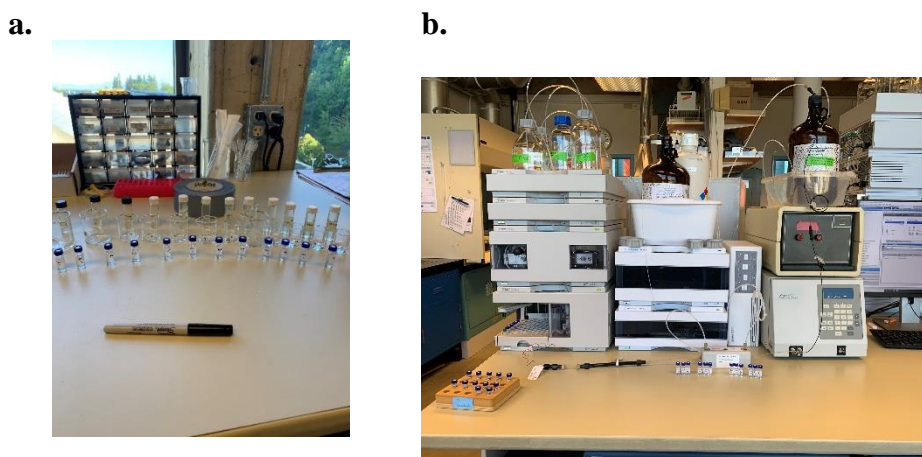
Figure 12. Sulfate sample preparation (a) and HPLC instrument (b).
2.2.3. Carbon Equivalent Calculation

Methane emission estimates are typically reported in "gCH_4 m^{-2} yr^{-1}" which are not comparable

to carbon storage units (typically in gC m^{-2} yr^{-1}). I used equation 1 to convert methane emission

estimates into "CO_2-equivalent greenhouse gas flux" to compare with sequestration rates. This

will ultimately allow me to compare carbon storage and the carbon emission potential of the

restored area of Port Susan Bay. Equation 1 below uses a global warming potential (GWP) of 25

to convert methane to a carbon dioxide equivalent (EPA 2021) and the weight fraction of carbon

in carbon dioxide to account for only carbon (12g of carbon in carbon dioxide).

$$\frac{gCH_4}{m^2 yr} \times \frac{25\ (GWP)}{} \times \frac{12g}{44g} = \frac{gC}{m^2 yr}$$

Equation (1)

2.2.4. Statistics

Statistical analyses and plots were done in R Version 4.1.2. I used rank-based Spearman

correlations to assess the direction and strength relationships between each variable listed in

table 3. Correlations were calculated using regression lines as pair-wise comparisons between

variables. The Spearman rank-based correlation method accounts for non-normal data.

Table 3. Variables used to calculate Spearman correlations.

Salinity & Sulfate	**Salinity** & Sed Temp	**Salinity** & pH	**Salinity** & Redox 2.5cm	**Salinity** & Redox 15cm	**Salinity** & Pooled Redox
	Sulfate & Sed Temp	**Sulfate** & pH	**Sulfate** & Redox 2.5cm	**Sulfate** & Redox 15cm	**Sulfate** & Pooled Redox
		Sed Temp & pH	**Sed Temp** & Redox 2.5cm	**Sed Temp** & Redox 15cm	**Sed Temp** & Pooled Redox
			pH & Redox 2.5	**pH** & Redox 15cm	**pH** & Pooled Redox
				Redox 2.5cm & Redox 15cm	**Redox 2.5cm** & Pooled Redox
					Redox 15cm & Pooled Redox

I used multidimensional scaling (MDS) to calculate a stress value and assess how similar the

sites are. Analysis of similarity (ANOSIM) was also used to determine site discrepancies and the

Similarity percentages (SIMPER) analysis was used to calculate percent contribution of each

variable to site similarities. Data were normalized between zero and one before conducting

MDS, ANOSIM, and SIMPER analyses. I also ran one-way ANOVA and Tukey HDS tests to

determine significant differences in redox depth data and vegetation composition.

2.3. Results

2.3.1. Salinity

Salinity was highest in the summer months and nearly zero in the February 2021 (Figure 13). These results represent an average over the depth of the sampling pits. The highest average salinity was 17.6ppt (±1.4) at RM1 in August 2020 and the lowest was 0ppt (±0) at RS1 and RS2 in February 2021. Salinity in the summer months was more variable between replicate sites than in the winter; at RM1 in August 2020, salinity ranged from 15ppt to 20ppt between the three replicate sites. There was less variation in October 2020, February 2021, May 2021, and June 2021 with nearly all standard errors below 1ppt. RM1 and RM2 had consistently higher salinities than RS1 and RS2 throughout the project duration, with the most separation in August 2021.
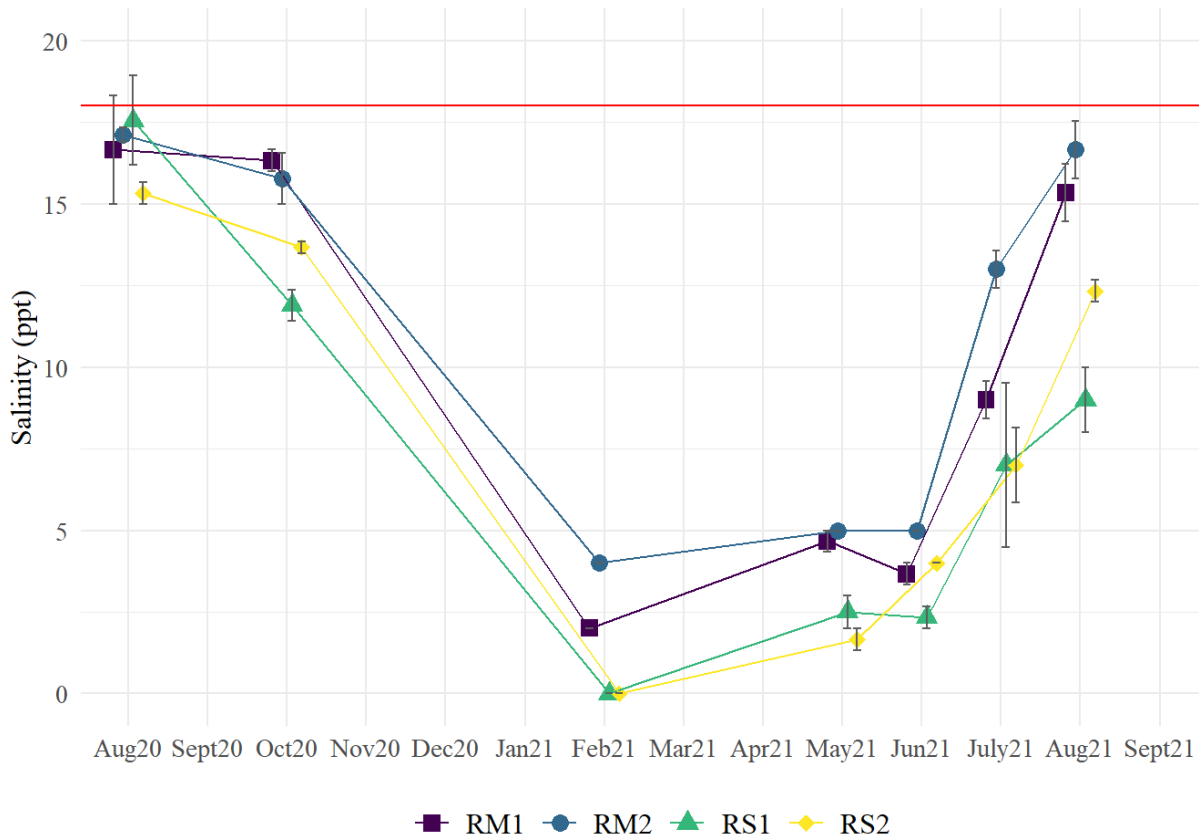
Figure 13. Salinity (in ppt) at RM1, RM2, RS1, and RS2 in Port Susan Bay, WA with standard error. Salinity calculated as average of three replicates per site.

2.3.2. Sulfate

Sulfate concentrations followed trends in salinity; sulfate was higher in the summer and low in the winter (Figure 14). There was more variability in the summer months than in the winter. The highest sulfate concentration was 2032.5ppm (±1200) at RM1 in August 2020. The sulfate concentrations recorded in August 2020 were highly variable and considerably higher than all other measurements. The next highest sulfate concentrations, other than in August 2020, were in August 2021. In August 2021 the highest sulfate concentration was 609.2ppm (±121) at RM1 and 602.4ppm (±53) at RM2. RS1 and RS2 generally had lower sulfate concentrations except for in June 2021. Sulfate concentrations were very low at RS1 and RS2 in February 2021 and May 2021 (52.2ppm±8, 66.0ppm±19, 24.9ppm±10, and 56.4ppm±20 respectively).

26

Figure 14. Sulfate (in ppm) at RM1, RM2, RS1, and RS2 in Port Susan Bay, WA with standard error. Sulfate calculated as average of three replicates per site.

2.3.3. Sediment Temperature

The highest sediment temperature was measured at RM2 in June 2021 at 21.5°C (±0.35). The lowest temperatures were at RS1 and RS2 in February 2021 (both 3.4°C ±0.06 and ±0.07 respectively, Figure 15). The seasonal trends in sediment temperature also generally followed that of salinity and sulfate. Additionally, RS1 and RS2 had lower temperatures than RM1 and RM1 from February 2021 through the end of the project. There was little variability in sediment temperature measurements at each site. Despite more replicates than salinity and sulfate the greatest variability was 0.35°C at RM2 in June 2021 and the lowest was 0.01°C at RM1 in February 2021.
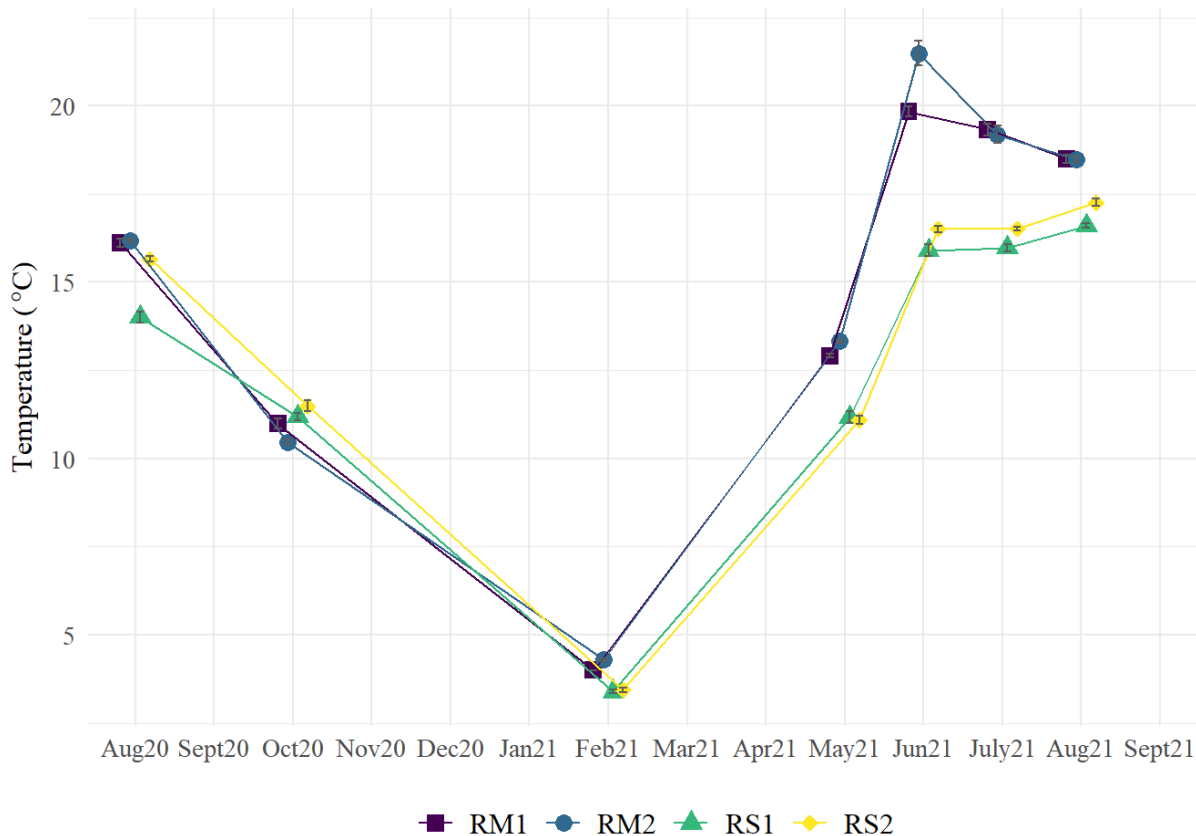
Figure 15. Sediment temperature (in °C) at RM1, RM2, RS1, and RS2 in Port Susan Bay, WA with standard error. Sediment Temperature calculated as average of nine measurements per site.

2.3.4. Redox

Pooled average redox values were between 0mV to 300mV; within the iron and nitrogen reduction range (Mitsch and Gosselink, 2015). Redox was fairly consistent throughout the year and there were no clear patterns among the sites . The highest average redox was at RM2 in February 2021 (228.0mV±16) and the lowest was at RM1 in June 2021 (58.5±54) (Figure 16). Redox readings were more variable in the summer months. Before correcting for calomel electrode potential, the redox values ranged from -236.0mV to 638mV.

When separated by depth (average of all four sites), redox is higher at 2.5cm deep than at 15cm (Figure 17). Interestingly a one-way ANOVA revealed that redox at 2.5cm and 15cm is significantly different when all the data are pooled ($F_{1,348}= 40.85$, $p<0.001$). It is only

28

significantly higher at 15cm in May 2021, June 2021, and August 2021 (ANOVA results: $F_{1,45}=$ 13.19, p<0.001 and; $F_{1,46}=$ 19.97, p<0.001 and; $F_{1,46}=$ 6.30, p=0.02 respectively). Redox at 2.5cm and 15cm was most different in June 2021 and most similar in February 2021.
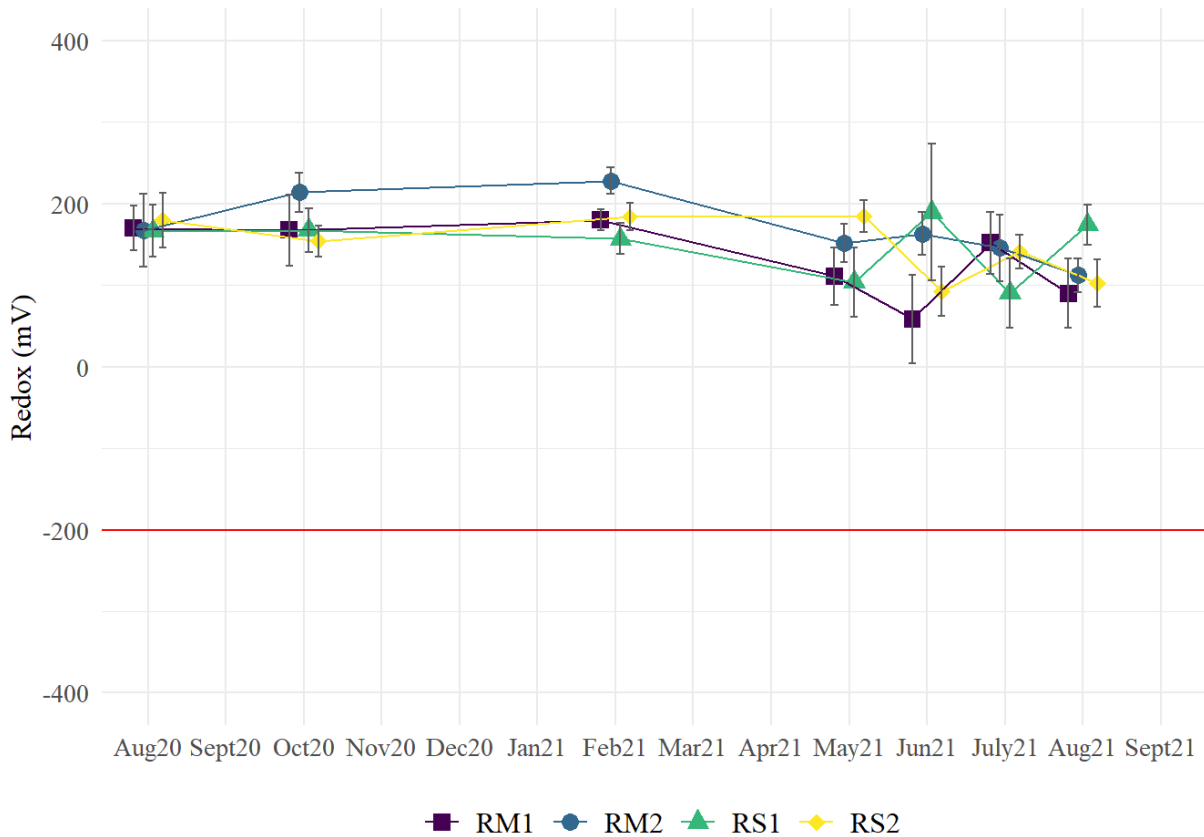
Figure 16. Redox (in mV) at RM1, RM2, RS1, and RS2 in Port Susan Bay, WA with standard error. Redox calculated as average pooled values from 2.5cm and 15cm depth at each site. Red line indicates redox potential at which sulfate reduction begins. See Appendix E for number of electrodes used at each depth during each sampling period.
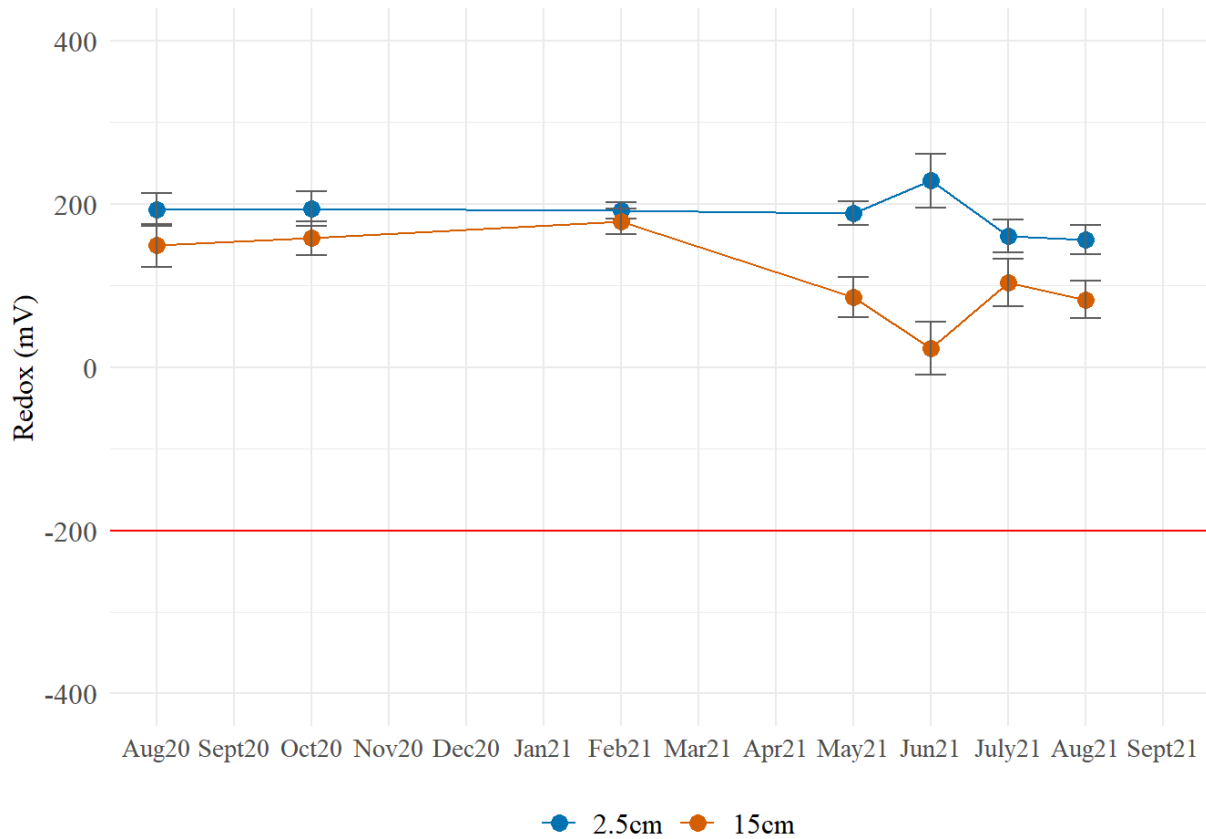
Figure 17. Redox (in mV) at 2.5cm and 15cm depth in Port Susan Bay, WA with standard error. Redox calculated as the average pooled values for all four sites at 2.5cm and 15cm depth. Red line indicates redox potential at which sulfate reduction begins. See Appendix E for number of electrodes used at each depth during each sampling period.

2.3.5. Vegetation Composition

Average vegetation percent cover was highest at RS1 and RS2, at or close to 100% during the summer months (Figure 18). RM1 and RM2 had lower vegetation cover but saw an increase from summer 2020 to summer 2021. The dominant, and only, species found at RS2 in August 2021 was *Typha angustifolia* (82%) (Figure 19 & 20b, Appendix H). RS1 also had *Typha angustifolia* (28%), but the primary species present was *Carex lyngbyei* (57%) (Figure 19 & 20a, Appendix H). RM1 was dominated by *Bolboschoenus maritimus* (78%) and RM2 was dominated by *Schoenoplectus pungens* (47%) in August 2021 (Figure 19, 20c, & 20d. Appendix H). Matted algae were also present on bare sediment at RM1 and RM2. RM1 and RM2 had similar species composition as did RS1 and RS2.
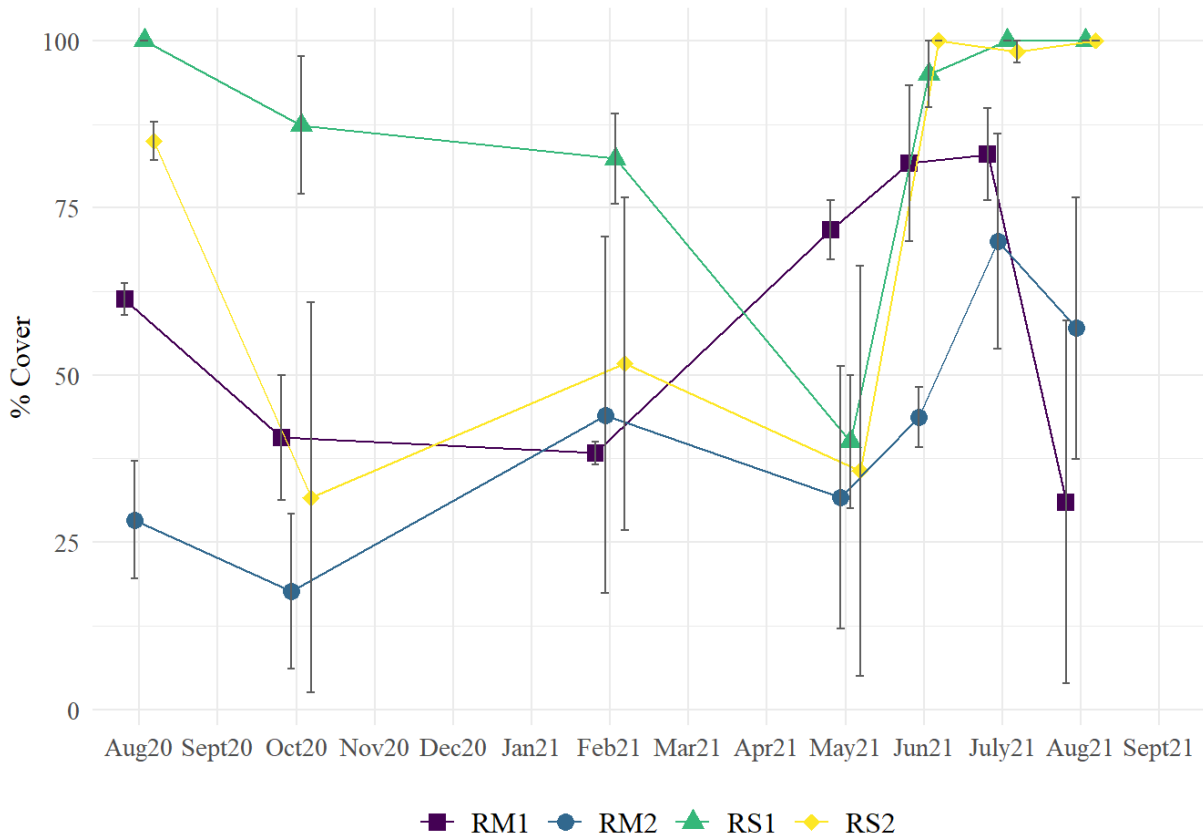
Figure 18. Average vegetation percent cover at RM1, RM2, RS1, and RS2 in Port Susan Bay, WA with standard error. Percent cover calculated as average total percent cover (of all species) at each replicate site.
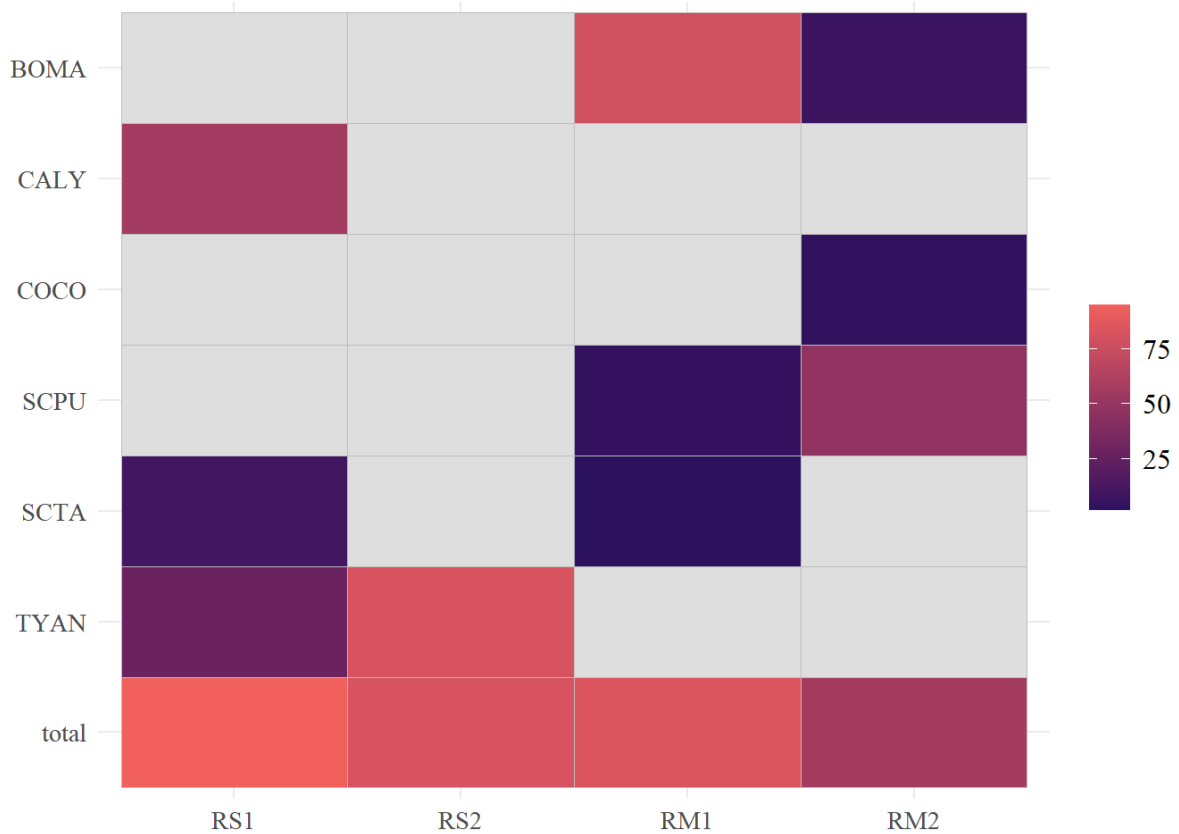
Figure 19. Vegetation composition (percent cover) of dominant species at RM1, RM2, RS1, and RS2 in Port Susan Bay, WA in August 2021. Species codes are as follows: BOMA; *Bolboschoenus maritimus*, CALY; *Carex Lyngbyei*, COCO; *Cotula coronopifolia*, SCPU: *Schoenoplectus pungens*, SCTA; *Schoenoplectus pungens*, TYAN; *Typha angustifolia*.
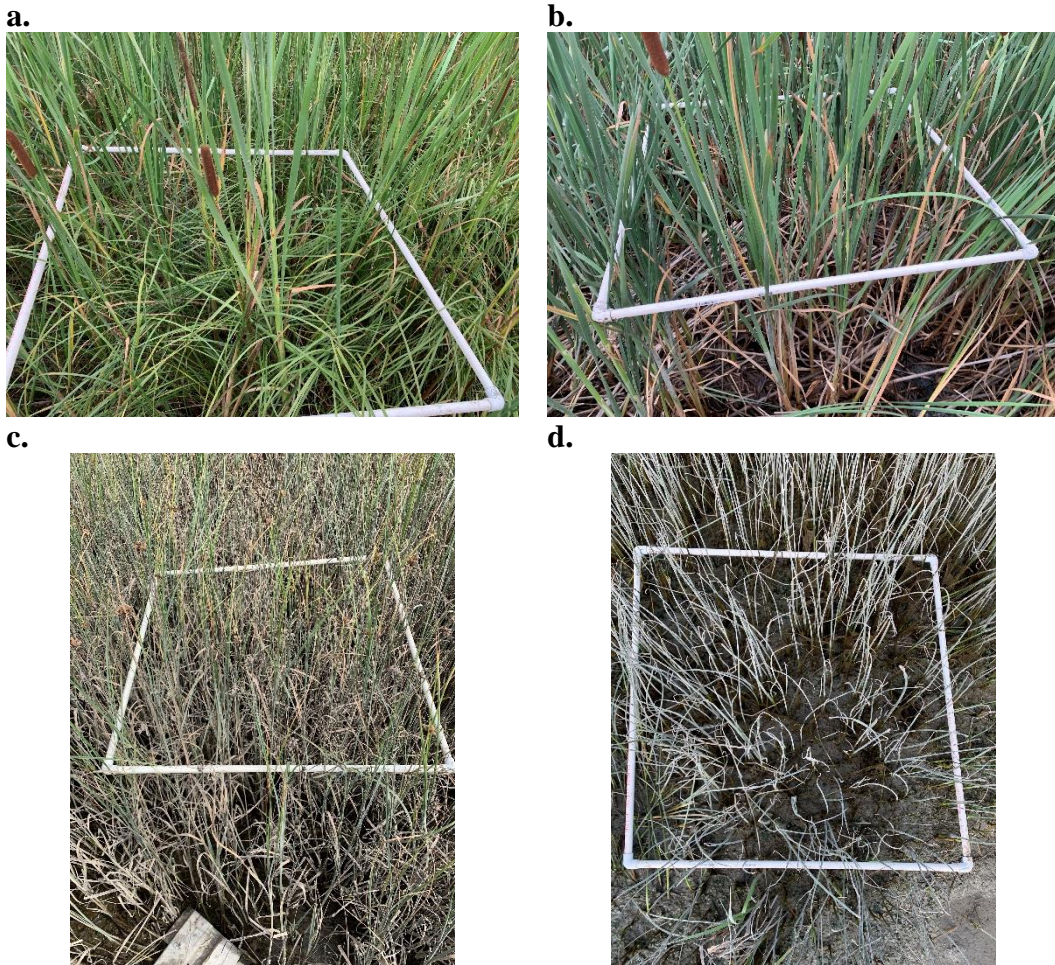
Figure 20. Vegetation quadrats at one replicate site representative of *Typha angustifolia* and *Carex Lyngbyei* at RS1 (a), *Typha angustifolia* at RS2 (b), *Bolboschoenus maritimus* at RM1 (c) and *Schoenoplectus pungens* at RM2 (d) in Port Susan Bay, WA August 2021.

2.3.6. Biomass

Biomass (gdw/m^2) increased 234% from 2016 to 2020 based on an average of the four sites within the restoration area (Figure 21a). RS1 had the highest end of season biomass, and the highest variability among the three replicate sites in 2020 (2223±158gdw/m^2) (Figure 21b). RS1 was closely followed by RS2 (1959±13gdw/m^2) (Figure 20b). RM1 and RM2 bad biomass nearly an order of magnitude lower than RS1 and RS2 (RM1: 417±19gdw/m^2 and RM2:112±17gdw/m^2 respectively) (Figure 21b). Biomass was significantly different between sites in August 2020 ($F_{3,8}$= 11.09, p=0.003). Tukey HSD reveals that RM1 and RM2 are not significantly different from each other (p=0.90, 95% CI=[-439, 287]), and neither are RS1 and RS2 (p=0.93, 95% CI=[-429, 297]). All other site combinations are significantly different from one another (p<0.05).
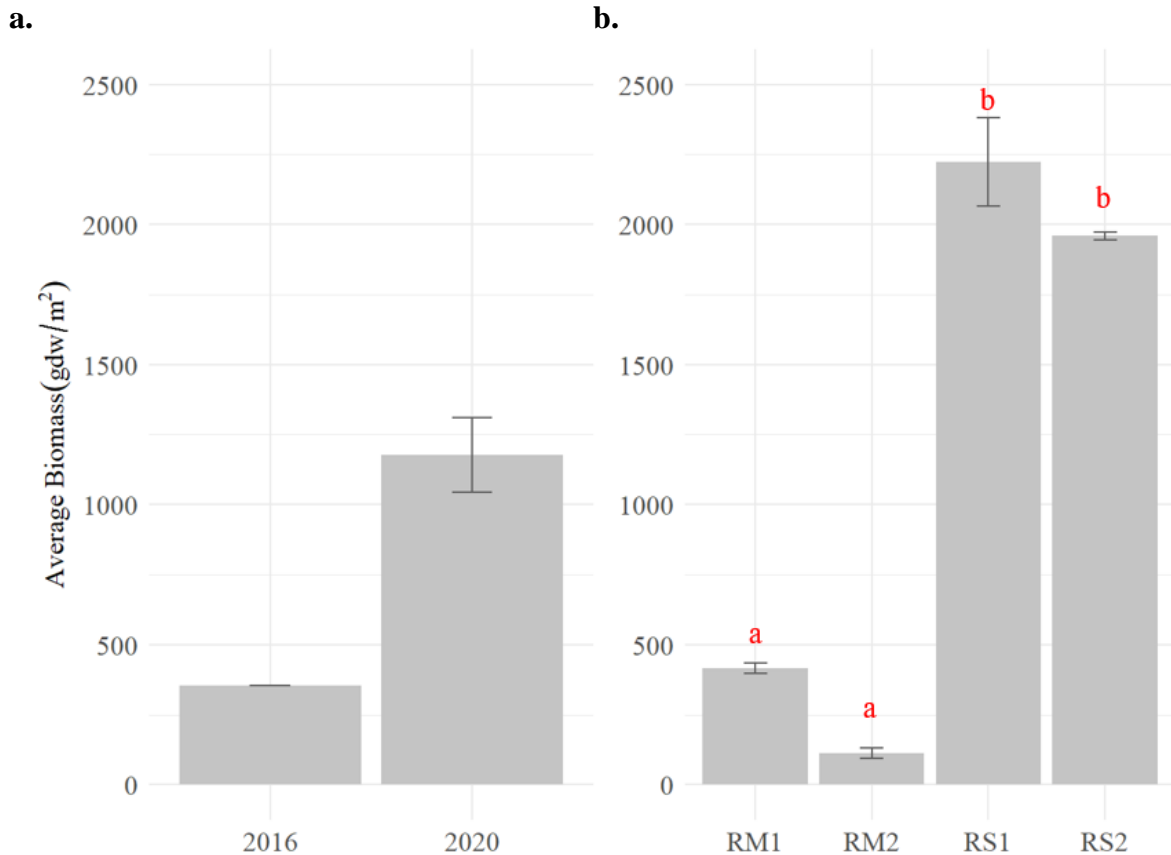
Figure 21. End of season biomass (gdw/m^2). Average biomass calculated as average of RM1, RM2, RS1, and RS2 and 2016 data from Poppe & Rybczyk 2021 (a), and 2020 average end of season biomass at each site (b). Letters denote significant differences.

2.3.7. Hydrogen Sulfide

Hydrogen sulfide was measured in August 2021. All measurements were between 0ppm and 7ppm. RS1 and RS2 appear to have lower average measurements than RM1 and RM2 (0±0, 1.7±1.7, 0±0, and 4±2.1 respectively).

2.3.8. pH

pH was generally lowest at RS2 and highest at RM2 (Figure 22). The highest average value was 7.4 (±0.23) at RM2 in June 2021 and the lowest average value was 6.1 (±0.06) at RS1 in July 2021. The highest variability was measured at RM2 and the lowest at RS1. Although all average pH measurements were between pH values of 6 and 7.5, there were clear groupings between RM1 and RM2 and RS1 and RS2. The two groupings were most different in June and July 2021 (largest difference 1.3 pH units) and converged in August 2021 within 0.7 pH units of each other.
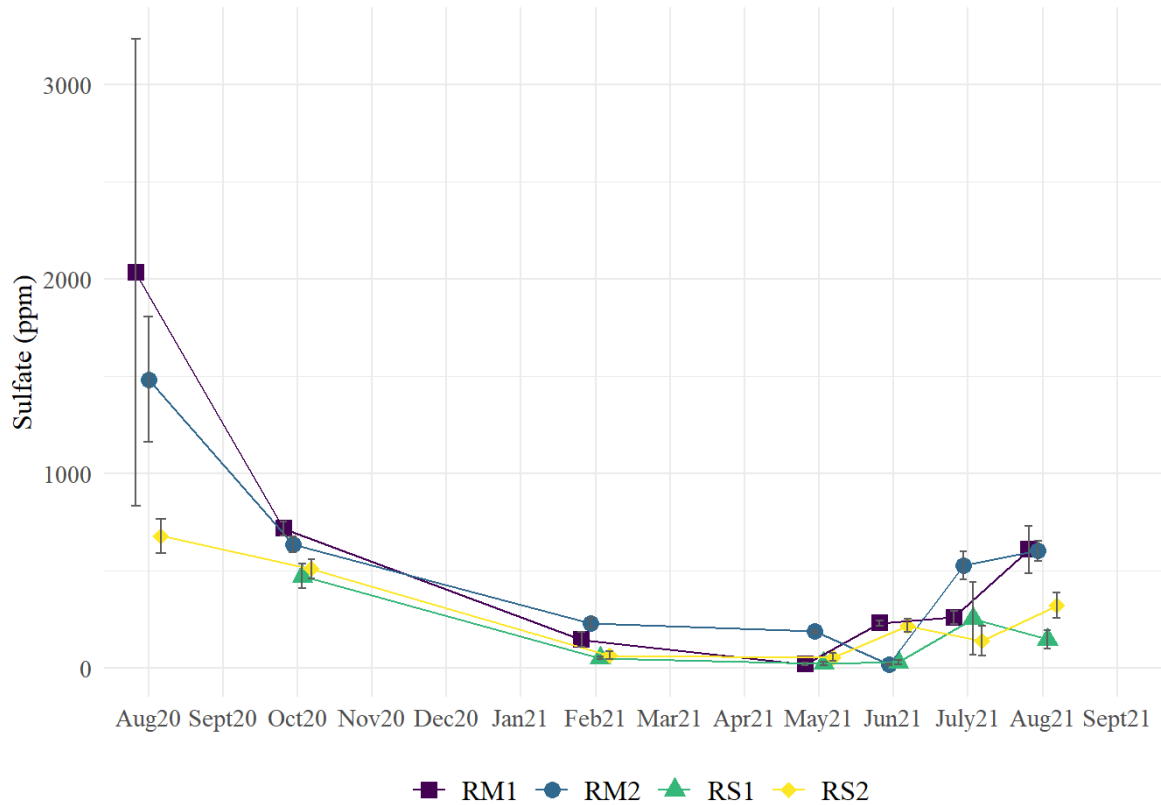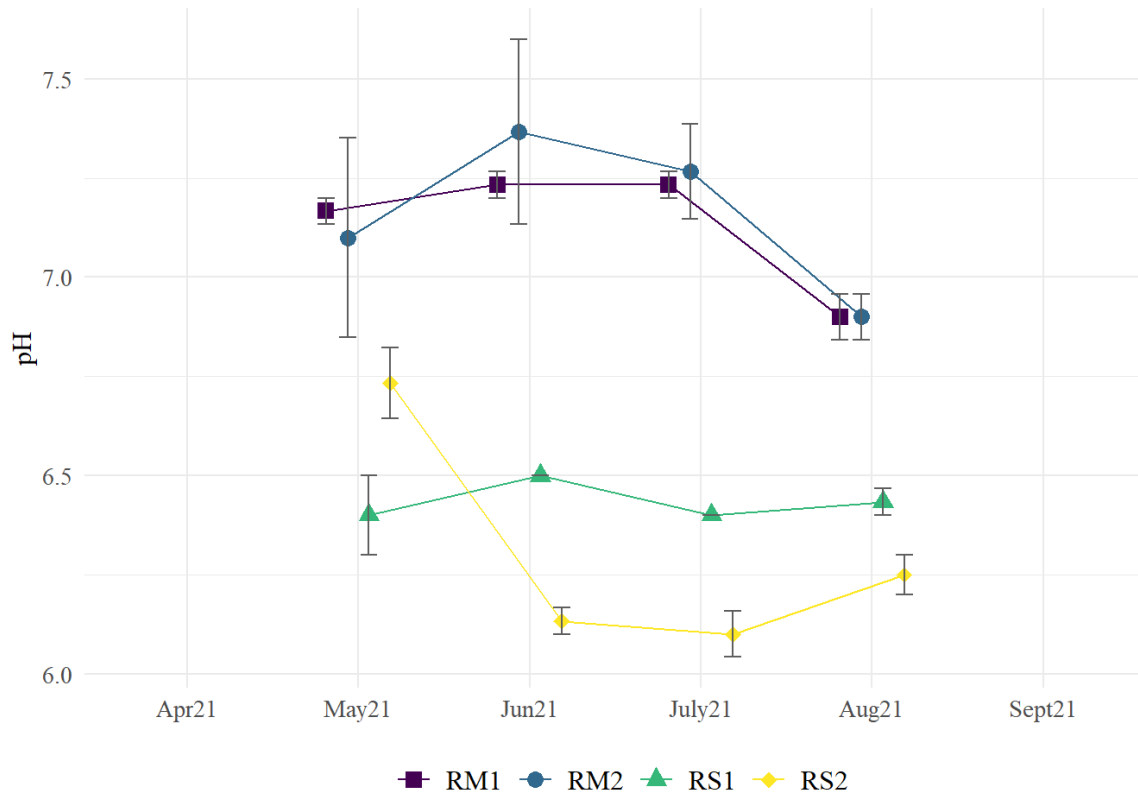

Figure 22. pH at RM1, RM2, RS1, and RS2 in Port Susan Bay, WA with standard error. pH calculated as average of three replicates per site.

2.3.9. Correlations

I classify a "strong" correlation as r-values greater than 0.5 or less than -0.5. Salinity and sulfate had the strongest overall positive correlation (r=0.76) (Figure 23 and Appendix D). When broken down by site, RS2 had the strongest correlation followed by RS1, RM2, and RM1 (r=0.92, r=0.88, r=0.80, and r=0.75 respectively). Salinity also had strong correlations with sediment temperature at RS2 (r=0.56), pH at RM1 (r=-0.52) and RS2 (r=-0.51), and 15cm redox at RS1 (0.78) (Figure 23).

pH has a strong positive correlation with pooled redox (by depth) at RM2, RS1, and RS2 (r=0.64, r=0.88, and r=0.80 respectively). Interestingly, this pattern is seen in 2.5cm redox (RM1: r=0.80, RS1: r=0.98, RS2: r=0.79) and not so much in 15cm redox; only RS2 had a strong positive correlation (r=0.67) while the other sites had weak correlations (RM1=0.05, RM2: 0.39, and RS1: -0.36).
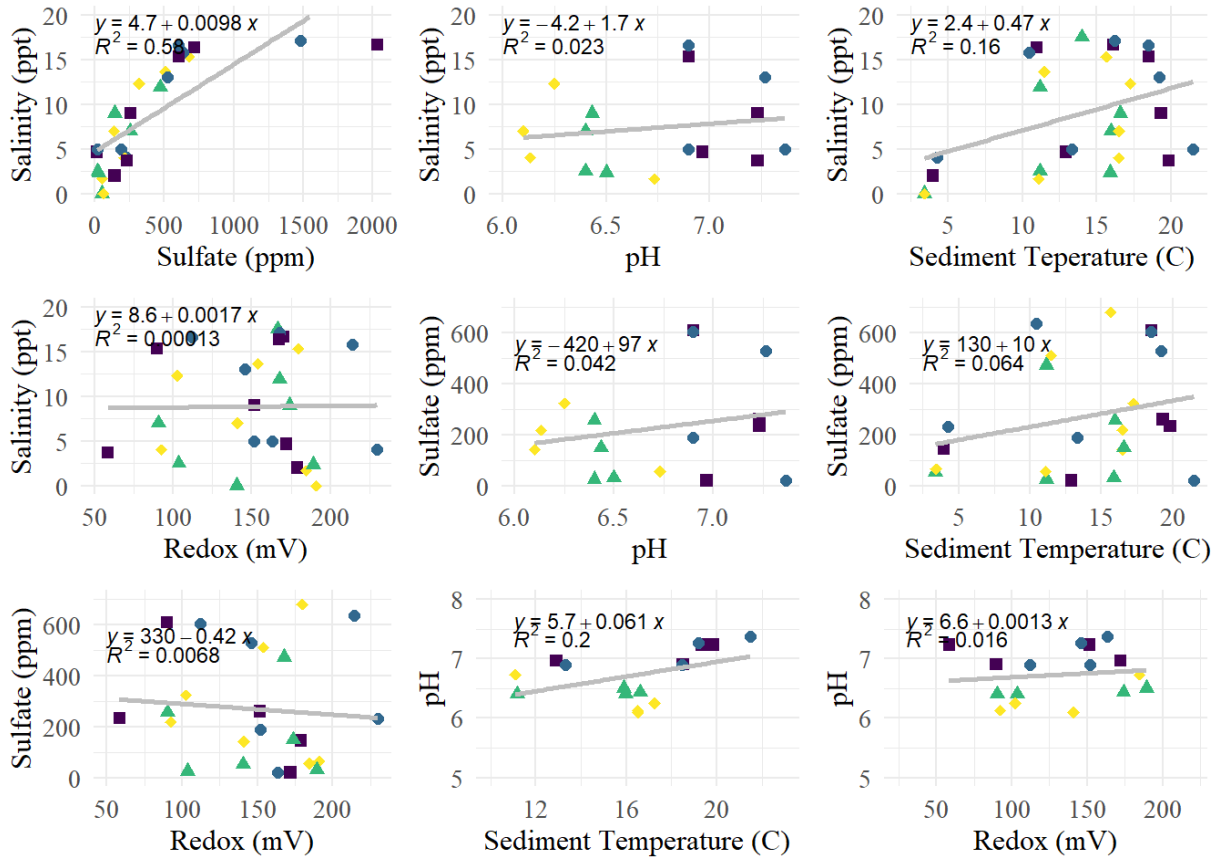
Figure 23. Scatter plots of pairwise comparisons of each variable tested. Regression line and R^2 reported based on pooled data for all four sites (RM1, RM2, RS1, and RS2). Correlations calculated by taking the square root of R^2 values. Colors and shapes denote site; purple squares: RM1, blue circles: RM2, green triangles: RS1, and yellow diamonds: RS2.

2.3.10. Site Characterization

As observed above, the sites tend to group based on location within the restored area at Port Susan Bay, WA. RS1 and RS2, at the south end of the restored area, generally have lower salinity, sulfate, and sediment temperature as well as higher vegetation cover than RM1 and RM2 (Figure 24).

Contrary to the observed differences above, stress, calculated through multidimensional scaling, suggests weak ordination groupings between sites (stress=0.145, supplementary Appendix F). ANOSIM results also show that the sites are quite similar (R=0.11, p=0.002). The SIMPER analysis between sites revealed that the combination of vegetation percent cover and salinity

accounts for nearly 50% of the average difference between RS2 and RM1, RS2 and RM2, RM1 and RS1, and RM2 and RS1.
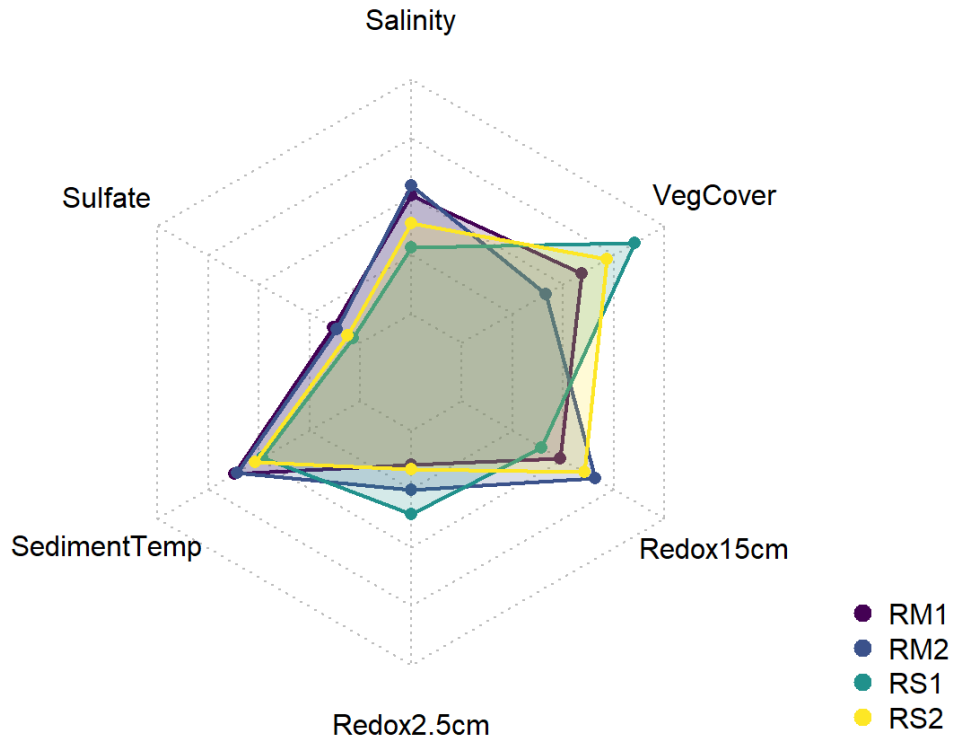
Figure 24. Radar plot depicting relationship between each site (RM1, RM2, RS1, and RS2) and variables (salinity, vegetation cover, redox at 15cm, redox at 2.5cm, sediment temperature, and sulfate). All variables were normalized before plotting for equal axes from 0 (center) to 1 (outer "web").

2.4. Discussion

2.4.1. Environmental Data Trends

While coastal wetlands have the ability to sequester blue carbon, they can also release greenhouse gases from anoxic environments. The interactions between environmental factors paint a complex picture of potential emissions from this location. Environmental factors measured indicate low or negligible methane emissions throughout the restoration area of Port Susan Bay. The combination of conditions that would indicate high methane emissions, such as low salinity and high pH, are typically accompanied by other environmental conditions that may counterbalance these affects (e.g. low sediment temperature). Even the best evidence for methane emissions in Port Susan Bay (i.e. late summer at RS1 and RS2) may be offset by redox potential and vegetation. Average redox alone does not drop below -100mV suggesting that more energetically favorable terminal electron acceptors than carbon dioxide or even sulfate are being reduced year-round.

In the following sections I will discuss each factor in turn.

2.4.1.1. Redox

Annual trends in redox potential alone suggest that methane is not being produced at any of the sites in Port Susan Bay, WA. Average redox is well above -200mV, the redox potential at which carbon is reduced to methane in sediments (Mitsch and Gosselink 2015). Redox potential results suggest that nitrate, manganic and ferric iron are being reduced in these sediments; all are more energetically favorable than sulfate (reduced at redox potentials ranging from -100mV to -200mV, Table 1).

2.4.1.2. Salinity and Sulfate

Salinity and sulfate were well correlated (R=0.76). Salinity is commonly used as a methane indicator, but sulfate concentrations are a more direct indicator because microbes that reduce sulfate can outcompete methane reducers. Poffenbarger et al. (2011) reports negligible methane emissions at sulfate concentrations above 4mM (approximately 384ppm). Sulfate concentrations were below 4mM during most of the study with the exception of August 2020, August 2021 and October 2021. Additionally, salinity was near 18ppt during these months at most of the sites indicating minimal methane emissions (Poffenbarger et al. 2011). While low salinity and sulfate in the spring and winter months (Figure 25) may be conducive to methane emissions, the low sediment temperature and low pH likely suppress any notable emissions.

Decoupling between salinity and sulfate suggests that there may be some localized sulfate depletion at intermediate salinities. Figure 25 shows that most of the salinity to sulfate ratios observed in this study are below the expected seawater ratio of sulfate to salinity. This is why it is important to measure sulfate concentrations alongside salinity because the actual proportions may not follow the rule of constant proportions as inferred in some studies. Despite redox conditions that do not suggest sulfate reduction, localized areas of sulfate depletion may suggest otherwise. This, however, does not necessarily mean that methane was being produced in these sediments.
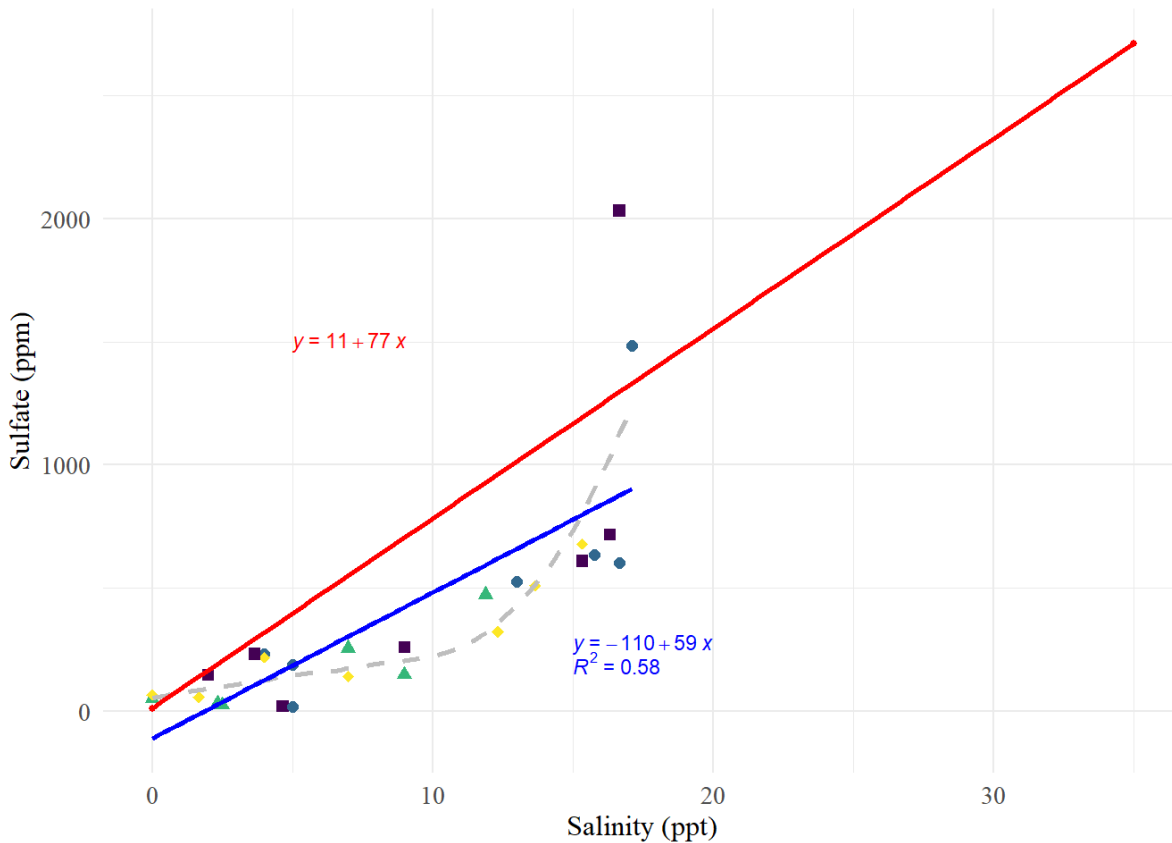
Figure 25. Average salinity (ppt) and sulfate (ppm) in Port Susan Bay, WA with seawater salinity to sulfate mixing ratio in red. Seawater sulfate and salinity values reported from Mitsch and Gosselink (2015). Blue line represents linear regression of Port Susan salinity and sulfate data. Gray dashed line depicts loess smoothing line of Port Susan salinity and sulfate data.

2.4.1.3.   Sediment Temperature

Schultz (2019) reported low methane emissions at soil temperatures below 15°C along the

Oregon coast. Average sediment temperature in Port Susan Bay, WA was only greater than 15°C

during Summer months, most of which coincided with high salinity and sulfate concentrations.

June and July 2021 were an exception because of high temperatures and low salinity and sulfate.

Methane emissions could occur during these months, particularly at RS1 and RS2 where salinity

and sulfate were lower. Despite sediment temperatures and sulfate concentrations conducive to

methanogenesis, redox conditions higher than -200mV still favored other metabolic pathways.

There is conflicting information on whether or not temperature can be a strong predictor of methane emissions. For example, Vizza et al. (2017) report seasonal variation in emissions, not necessarily from temperature alone. Additionally, Al-Haj and Fulweiler (2019) report temperature as a poor predictor of methane dynamics despite high emissions in warm seasons. Rather, Al-Haj and Fulweiler (2019) suggest a more holistic approach to assessing emissions using a more robust suite of environmental parameters. This sentiment aligns with the environmental data collected in this study. While many factors (e.g. high sediment temperature) may suggest high methane emissions, other factors consistently suggest otherwise (e.g. redox).

2.4.1.4.   pH

Wang et al. (1993) found that neutral pH is optimal for methane production. Slight deviations from neutral impact methane production; a decrease suppresses production, and an increase of about 0.2 enhances production (Wang et al. 1993). pH was close to neutral (pH=7) throughout the year in the restoration area. It was consistently slightly higher at RM1 and RM2 than at RS1 and RS2, although all within about one unit. The combination of lower pH and high redox values at RS1 and RS2 likely outweigh the other factors that suggest methane emissions at these sites during the summer months. RM1 and RM2 have pH levels above neutral suggesting enhanced methane production; however, these sites have consistently high redox and sulfate.

2.4.1.5.   Vegetation, Biomass, and Organic Matter

Literature on how vegetation species composition affects methane emissions is mixed because of site-specific conditions and a myriad of indirect effects. Plants can not only move gases through their vascular tissue, some plant traits are conducive to changing soil redox conditions (Muller et al. 2020). Further, shifts in vegetation composition, as a result of sea level, can mediate methane emissions (Muller et al. 2020). The vegetation surveys done at Port Susan Bay only account for

dominant species and provide a rough estimate of percent cover. A comprehensive look at how vegetation composition impacts methane emissions is beyond the scope of this project. However, the surveys illustrate functional groupings among the species observed at the four sites. These high-level groupings could help decipher if or how methane is being released or mitigated in these areas.

Both Kao-Kniffin et al. (2010) and Bhullar et al (2013) found graminoid species to have higher emissions than forbs. Specifically, Kao-Kniffin et al. (2010) found *Phalaris arundinacea* and *Typha angustifolia* to have lower emissions than *Carex stricta* and *Scirpus atrovirens*; where greater plant biomass was less conducive to methane emissions. Muller et al. (2020) reports that *Shoenoplectus* have a greater ability to oxidize the rhizosphere, and thus increase the redox potential, than *Spartina*. All four sites in the restoration area in Port Susan Bay are highly vegetated; RS1 dominated by *Typha angustifolia* and *Carex lyngbyei*, RS2 by *Typha angustifolia*, RM1 by *Bolboschoenus maritimus*, and RM2 by *Schoenoplectus pungens*. This suggests the potential for low methane emissions due to rhizosphere oxygenation based on limited data on similar plant species.

Biomass is an important consideration when assessing methane emissions as a function of vegetation species composition. Some studies generalize the relationship between plant biomass and methane emissions as being negative (e.g. Kao-Kniffin et al. 2010), others suggest that it is more species-specific. Generally, high plant biomass is conducive to higher rates of photosynthesis and rhizosphere oxidation. This trend is not true for all plant species due to various plant traits that affect redox conditions and plant mediated transport of methane to the atmosphere. Muller et al. (2020) found an inverse relationship between *Shoenoplectus* aboveground biomass and methane emissions and a positive relationship between *Spartina*

44

biomass and emissions. While average total vegetation percent cover was relatively high at all

four sites in the restoration area (RM1: 84%, RM2: 57%, RS1: 95%, and RS2: 82%), the biomass

at RM1 and RM2 versus RS1 and RS2 were significantly different. RS1 and RS2 had

significantly higher biomass ($417gdw/m^2$ and $112gdw/m^2$ respectively) than RM1 and RM2

($2223gdw/m^2$ and $1959gdw/m^2$ respectively). Additionally, average biomass increased 234%

from 2016 to 2020 within the restoration area. This increase in biomass in combination with the

specific plant species could suggest low emissions due the potential for rhizosphere oxidation.

Increased vegetation, while likely adding to the blue carbon stored in sediments, also contributes

to the organic matter used as a substrate source by microbes to produce methane. Vizza et al.

(2017) hypothesize that increased organic matter at the end of the growing season can contribute

to higher methane emissions. The organic matter in Port Susan Bay is relatively low, particularly

in the restoration area (Poppe and Rybczyk 2021) suggesting that there is limited substrate for

methane generation. Some marshes, such as one in coastal Louisiana, have organic contents

upwards of 50% (Lane et al. 2017) versus in the restored area of Port Susan Bay which has

4.93% (Poppe and Rybczyk 2021). Organic matter content may have increased since 2016 when

the cores to measure organic matter were taken due to the sharp increase in plant biomass.

2.4.2.   Methane Emission Estimation

There are several ways to infer estimates of methane emissions using the environmental datasets

discussed above. In the following sections I will estimate emissions in the restored area of Port

Susan Bay, WA using IPCC emission factors, and values published by Poffenbarget et al. (2011),

and default factors (summary of equations in Appendix C).

2.4.2.1.   IPCC Emission Factors

Methane emissions can be estimated using IPCC emission factors for "rewetted land previously vegetated by tidal marshes and mangroves". Emission factors are laid out in the 2013 IPCC Guidelines for National Greenhouse Gas Inventories specifically for wetlands (IPCC 2013). The tier one emission factors differentiate emissions based on salinity. The emission factor for salinities greater than 18ppt is 0kg CH_4 ha^{-1} yr^{-1}, and 193.7kg CH_4 ha^{-1} yr^{-1} (range: 10.95-5392) for salinities less than 18ppt. These values are based on several studies, including Poffenbarger et al. (2011). Based on the salinity data collected in Port Susan Bay, methane emissions would be 193.7kg CH_4 ha^{-1} yr^{-1} (19.37gCH_4 m^{-2} yr^{-1}) at all sites except for in the late summer when salinities are near 18ppt. This may be a very high estimate based on the large range of salinity values this value can be applied to.

2.4.2.2.   Poffenbarger et al. (2011) Published Values

Published values by Poffenbarger et al. (2011) are widely referenced in methane studies (e.g. Schultz et al. 2019, Woo et al. 2021, Janousek et al. 2021). Poffenbarger et al. (2011) summarize methane emission values from a range of salinities to determine the relationship between salinity and methane emissions, and to determine the salinity above which emissions are negligible. The data were obtained from published studies on vegetated tidal marshes where methane emissions were measured with static chambers. Poffenbarger et al. (2011) extended the review of published values with an original study done in a Maryland tidal wetland. Table 4 summarizes values reported by Poffenbarger et al. (2011). Based on these data, methane emissions would be approximately 16.4gCH_4 m^{-2} yr^{-1} in the restored area of Port Susan Bay. All sites in Port Susan Bay are mesohaline (5-18ppt) for most of the year with the exception of very cold Winter months.

Table 4. Published methane emission values from Poffenbarger et al. 2011

Salinity	Methane Emissions	Carbon Dioxide Equivalent
Salinity < 0.5ppt	$41.9gCH_4m^{-2}yr^{-1}$	$10.5MgCO_2\ ha^{-1}\ yr^{-1}$
Salinity 0.5-5ppt	$150\ gCH_4m^{-2}yr^{-1}$	$37.5MgCO_2\ ha^{-1}\ yr^{-1}$
Salinity 5-18ppt	$16.4\ gCH_4m^{-2}yr^{-1}$	$4.1MgCO_2\ ha^{-1}\ yr^{-1}$
Salinity >18ppt	$1.12\ gCH_4m^{-2}yr^{-1}$	$0.3MgCO_2\ ha^{-1}\ yr^{-1}$

2.4.2.3. VCS Default Factors

The VCS Methodology for Tidal Wetland and Seagrass Restoration developed default factors for

baseline and project scenarios based on values by Poffenbarger et al. (2011). These factors are

used when direct measurements are not feasible. The default factors for baseline and project

scenarios are appropriate for only high salinities (>18ppt) and range from $0.011t\ CH_4\ ha^{-1}\ yr^{-1}$

($1gCH_4\ m^{-2}\ yr^{-1}$) to $0.0056tCH_4\ ha^{-1}\ yr^{-1}$ ($0.51gCH_4\ m^{-2}\ yr^{-1}$) respectively. These estimates would

only be appropriate for instances of high salinity in the hot summer months, otherwise they are

not appropriate for estimating emissions in Port Susan Bay. This suggests that default factors

need to be extended to a wider range of salinities, even if that means reporting high estimates.

2.4.3. Study Limitations and Recommendations

Many of the estimation methods rely heavily on salinity to estimate methane emissions. More

accurate estimations require a more comprehensive set of ancillary data. Salinity may not serve

as a very accurate predictor of methane in areas where there is sulfate depletion; emission factors

at high salinities could underestimate emissions (Poffenbarger et al. 2011). As more studies

report greenhouse gas emissions in the Pacific Northwest coastal wetlands, better models can be

used to predict emissions in adjacent areas to incorporate more site-specific variables such as

redox, sediment organic matter, temperature, and vegetation. Carbon dioxide and nitrous oxide

are two additional greenhouse gases that should be considered when assessing the viability of

carbon credits. These greenhouse gases would provide a holistic estimate of outputs, rather than net carbon loss.

Samples should be taken in the northern part of the restored area to provide more spatially representative estimates of the site. If possible, monitoring of variables such as salinity, sulfate, and redox should be taken at different times during the tidal cycle and at night. In addition to the restoration area, the same environmental data should be collected in adjacent natural marshes to use as a comparison. While assessing the carbon budget of the restoration area has implications for carbon credits, the adjacent natural areas can also inform restoration effectiveness over time. In order to compare methane emission estimates with the sequestration rates reported in Chapter 3, the global warming potential (GWP) of methane is used to calculate the carbon equivalent. While GWP describes a pulse event, some may argue that using the sustained GWP (SGWP) may be more accurate. GWP and SGWP values are very different both from one another and through time. For example, the methane GWP over 20 years is 85 compared to 30 at 100 years and 96 versus 45 for SGWP (Neubauer 2021). The choice of GWP versus SGWP and over which time period will drastically change emission estimates and how they compare to sequestration rates. I used a GWP of 25 to calculate carbon equivalents in this project because it aligns with commonly cited data from Poffenbarger et al. (2011) and is within the range reported by the EPA.

3. 2021 UPDATED SET MEASUREMENTS

3.1. Introduction

Carbon accumulation rates are an important component in determining the carbon balance of any given system. Further, accumulation rates help inform the voluntary carbon market to assess restoration funding. Accumulation rates represent how much carbon is being stored. These rates are reported as "$gCm^{-2} yr^{-1}$" and are calculated as the product of carbon accretion and carbon density. Carbon accretion ($cm\ yr^{-1}$) can be calculated in several different ways, including with ^{210}Pb dating and by measuring relative elevation change. While ^{210}Pb-based accretion rates are more widely reported in blue carbon studies (e.g. Crooks et al. 2014), SETs provide an alternative method to determine carbon accumulation rates. SETs are leveling devices installed and left in the field to measure relative change in elevation over time (Cahoon, 2022). They can be used in disturbed areas where ^{210}Pb-based methods are not accurate.

Researchers at Western Washington University installed and monitor 21 SETs in Port Susan Bay, WA. They were installed between 2011 and 2014, with roughly four in each zone (figure 2) and are monitored annually. The elevation change rates measured from the SETs are used to calculate long-term sediment accretion and annual carbon accumulation rates. Poppe and Rybczyk (2021) measured both SET and ^{210}Pb-based accretion in Port Susan Bay. They developed a ^{210}Pb:SET ratio of 0.57 which can be applied to SET-based calculations to create an estimate of ^{210}Pb accretion. Additionally, Poppe and Rybczyk (2021) analyzed sediment characteristics as each of the 21 sites to determine carbon density. Carbon density ($gC\ cm^{-3}$) is calculated as the product of bulk density ($g\ cm^{-3}$) and percent organic content.

I used measurements from the 2021 field season to calculate updated carbon accumulation rates at each SET in Port Susan Bay. While I calculated carbon accumulation at each of the 21 SETS, I

used SET data at the restoration area measurements (RS1, RS2, RM1 and RM2) to compare with carbon emission equivalents to determine the average carbon balance of this site.

3.2. Methods

3.2.1. Field Methods

Field measurements at each SET are taken in the Spring. Elevation change measurements follow methods outlined by Lynch, et al. (2015).

The field equipment (Figure 26) is comprised of a permanent benchmark rod and a leveling device (the SET). The benchmark rod is driven into the sediment to the point of refusal; around 4-5m. This allows for long-term accretion rate measurements because it accounts for compaction of the accreted sediments.

During annual monitoring, measurements are taken using the leveling device and a set of pins. There are nine pins on one side of the SET used to measure relative elevation change. The pins are lowered to the sediment surface and measured from the leveling device to the top of the pin. A total of 26 readings are taken at each SET; the leveling device is rotated to four precise seaward positions at each site and all nine pins are subsequently measured.
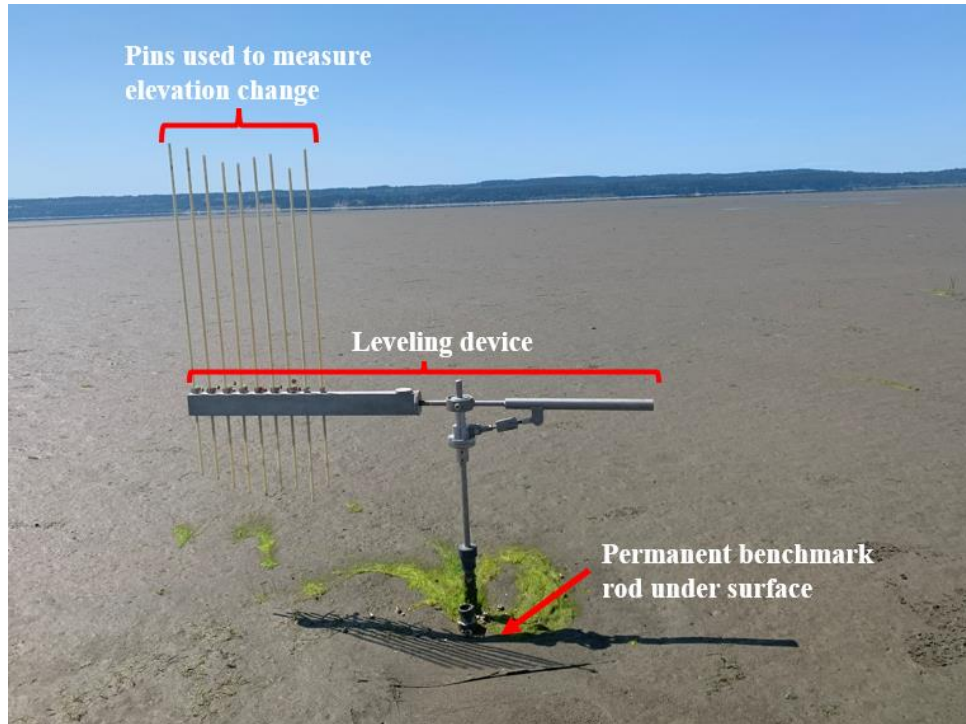
Figure 26. Field equipment set up at SET 5 in Port Susan Bay, WA.

3.2.2. Analyses

All calculations were done using the average of all pins per SET, per year (as fraction).

3.2.2.1. Elevation Change Rate

Before calculating elevation change rates, the elevation change relative to baseline needs to be calculated using the raw field measurements (Equation 2).

$$pin\ (cm) - baseline\ (cm) = elevation\ change\ relative\ to\ baseline\ (cm)$$
Equation (2)

Elevation change rates are then calculated using ordinary least square regressions for each SET (Figure 27), where the slope is the change rate (in cm yr^{-1}).
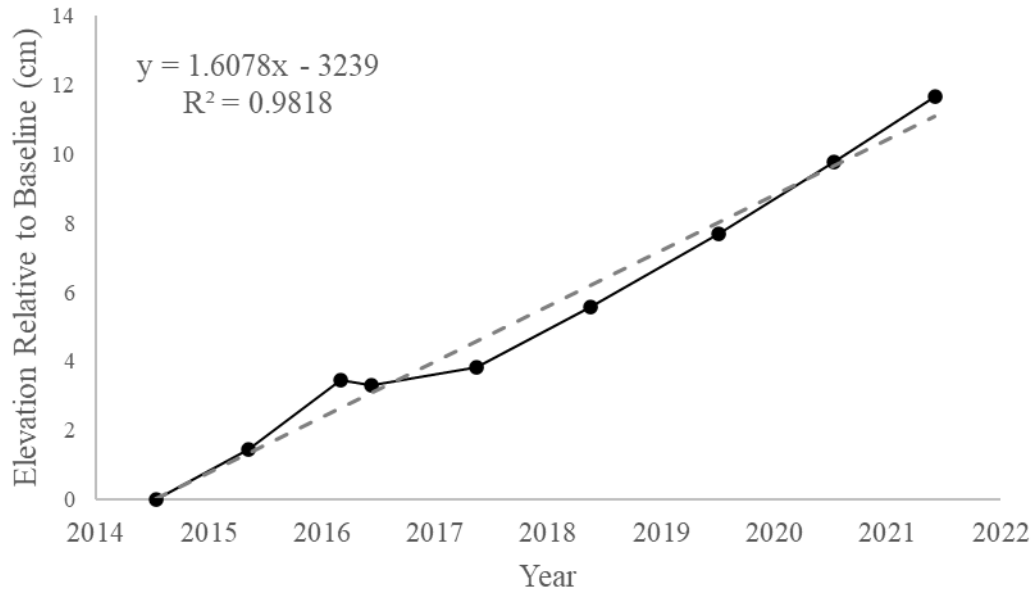
Figure 27. Example of elevation change rate (SET 27).

3.2.2.2. Carbon Accumulation Rate

Carbon accumulation rates for each SET are calculated as the product of the elevation change

rate (cm yr^{-1}) and the carbon density (gC cm^{-3}) at each site (Equation 3). Carbon density was

determined by Poppe and Rybczyk (2021) in 2016. The carbon densities that I used for my

carbon accumulation calculations were averaged for high and low marsh sites in each zone. The

restoration area (Zone 2) is an exception; there are two cores per SET in this zone. Accumulation

rates are reported in gC m^{-2} yr^{-1}.

$$elevation\ change\ rate\ \frac{cm}{yr} \times carbon\ density\ \frac{gC}{cm^3} \times \frac{1e^4 cm^2}{1m^2} = accumulation\ rate\ \frac{gC}{m^2 yr}$$
Equation (3)

To calculate long-term accretion rates comparable to ^{210}Pb, I multiplied the SET accumulation

rate by 0.57; the ^{210}Pb:SET ratio determined by Poppe and Rybczyk (2021). This is an average,

site-specific value used to correct for disturbed sediment in the restoration area and to create a

comparable value to other studies that use ^{210}Pb dating.

3.3. Results

3.3.1. Elevation Change Rates

The average elevation change rate (cm yr^{-1}) was 1.09cm yr^{-1} across all zones in Port Susan Bay, WA (Figure 2). Elevation change rate relative to initial is highest in the restoration area (Zone 2) followed by Zone 4 (Figure 28). The change rate is also highest in these two zones (2.46cm yr^{-1}±0.42 and 2.32 cm yr^{-1}±0.27 respectively, Figure 29 and Table 5). Zone 1 and Zone 3 appear to be plateauing with minimal elevation change in the past four years (0.80cm yr^{-1}±0.02 and 0.55cm yr^{-1}±0.11 respectively, Figure 28 and 29). Although Zone 5 still has a positive elevation change rate (0.31cm yr^{-1}±0.15, Table 5), it decreased in elevation from 2020 to 2021 (Figure 28). SET 5 which is denoted as "mud" (Figure 2) has the lowest elevation change rate (0.11cm, Figure 29) and initially subsided from the baseline (Figure 28).

Figure 30 shows the elevation change rate (calculated with linear regression) of each zone broken down by marsh type. The highest change rates are still seen in Zones 2 and 4, but the low marsh in Zone 4 has a higher change rate than the high marsh (Table 5).
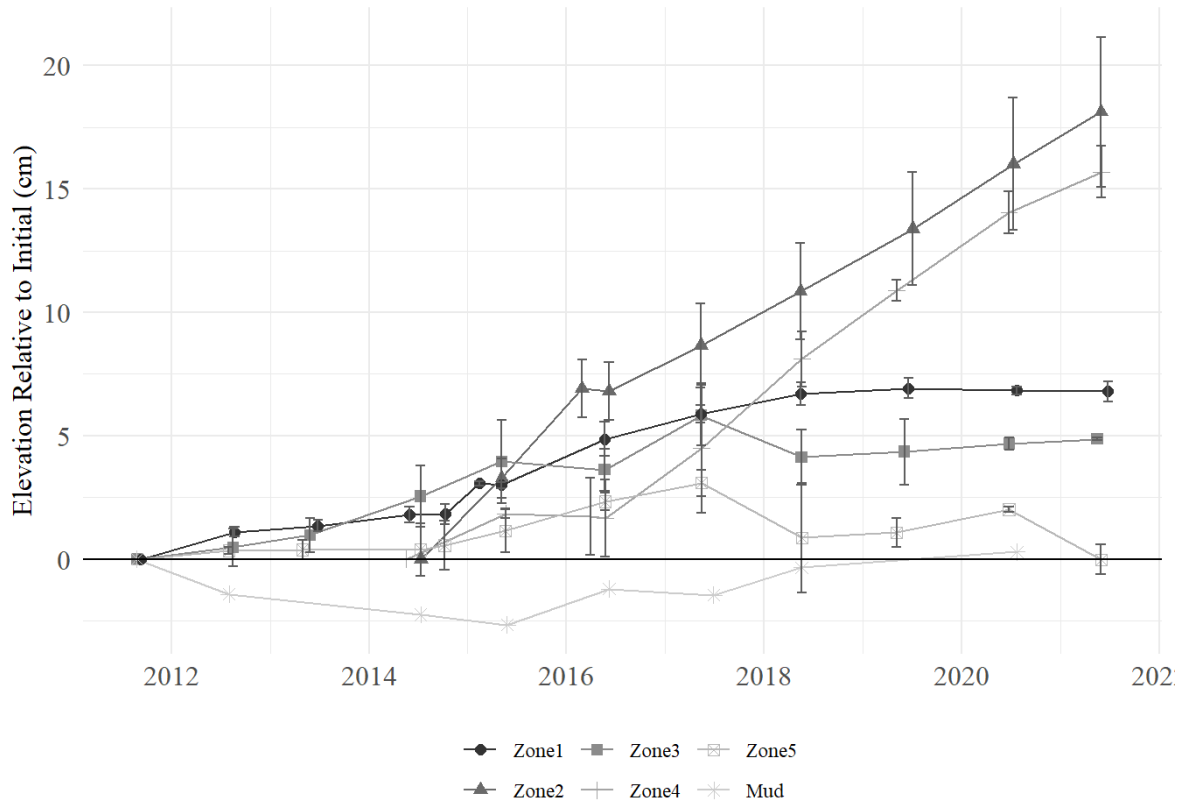
Figure 28. Elevation change relative to baseline (cm) over time in Port Susan Bay, WA with standard deviation. Zones are differentiated by shape. Horizonal line at "0" indicates baseline. Zone 2 is the restoration Zone. Zones 4 and 5 are natural marsh areas north of the restoration area, Zone 3 is west of the restoration area further into the bay, Zone 1 is a natural marsh across the Stillaguamish river south of the restoration area, and the "mud" site is beyond Zone 3.
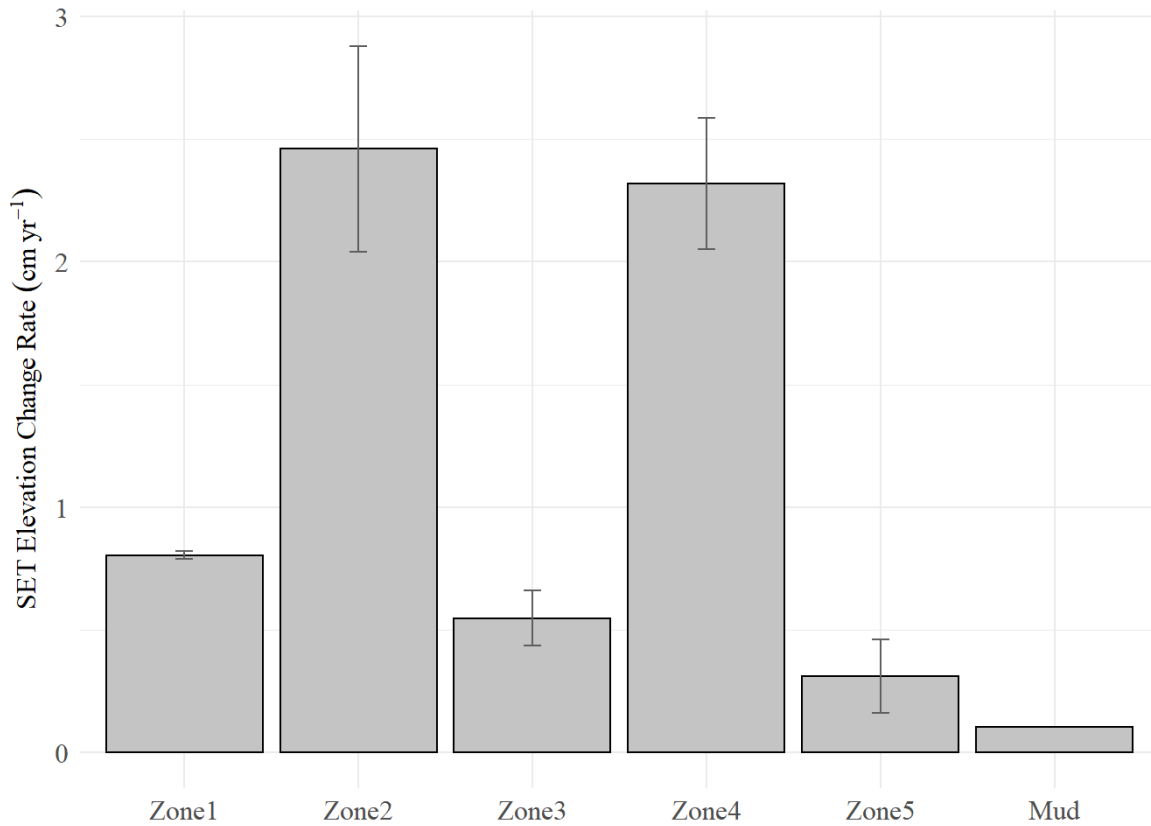
Figure 29. Elevation change rate by zone in Port Susan Bay, WA calculated as slope of elevation change over time with standard error.
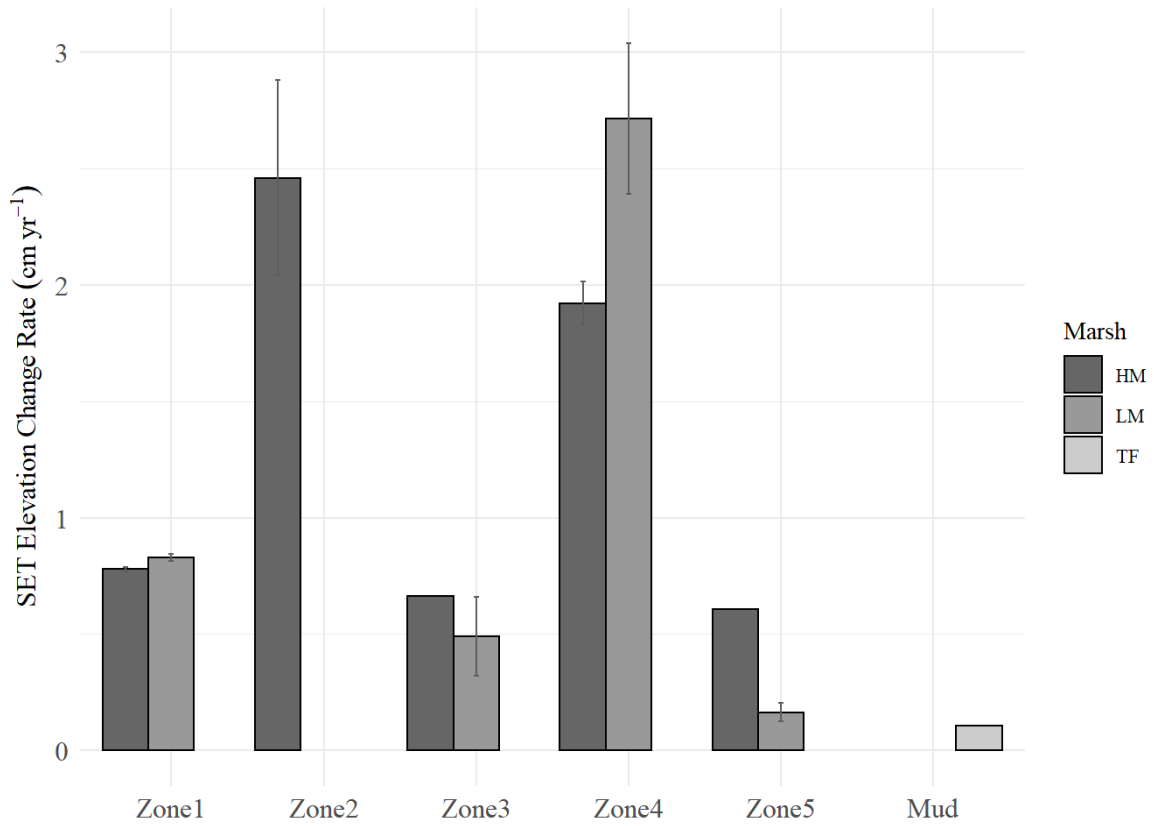
Figure 30. Elevation change rate broken down by marsh type for each zone in Port Susan, WA calculated as slope of elevation change over time with standard error. "HM" denotes high marsh areas, "LM" denotes low marsh areas, and "TF" is representative of the tidal flat or "mud" site.

Table 5. Elevation change and carbon accumulation rates (SET and Pb-based estimates) for all SETs and averages in Port Susan Bay, WA. "HM" denotes high marsh areas, "LM" denotes low marsh areas.

Site	SET ID	SET Elevation Change Rate (cm yr^{-1})	SET Carbon Accumulation Rate (gC m^{-2} yr^{-1})	Pb-based Carbon Accumulation Estimate (gC m^{-2} yr^{-1})*
HM5	2	0.61	157.87	89.99
LM5	3	0.20	32.50	18.52
LM5	4	0.12	19.94	11.36
LM5 mean		0.16	26.22	14.94
Zone 5 mean		0.31	70.10	39.96
HM1	7	0.77	153.78	87.65
HM1	8	0.79	157.86	89.98
HM1 mean		0.78	155.82	88.82
LM1	9	0.84	101.26	57.72
LM1	10	0.81	97.66	55.66
LM1 mean		0.83	99.46	56.69
Zone 1 mean		0.80	127.64	72.75
HM3	11	0.66	132.56	75.56
LM3	13	0.32	64.52	36.78
LM3	16	0.66	131.88	75.17
LM3 mean		0.49	98.20	55.97
Zone 3 mean		0.55	109.65	62.50
HM4	21	2.01	463.01	263.92
HM4	22	1.83	420.76	239.83
HM4 mean		1.92	441.89	251.88
LM4	23	3.04	608.10	346.62
LM4	24	2.39	478.36	272.67
LM4 mean		2.72	543.23	309.64
Zone 4 mean		2.32	492.56	280.76
Mud	5	0.11	10.52	6.00
RM2	25	3.20	416.64	237.48
RM1	26	3.16	505.17	287.95
RS2	28	1.87	298.98	170.42
RS1	27	1.61	225.09	128.30
Zone 2 mean		2.46	361.47	206.04

*Pb-based Carbon Accumulation Estimate calculated using [210]Pb:SET ratio (0.57) determined by Poppe and Rybczyk (2021)

3.3.2. Carbon Accumulation Rates

Average carbon accumulation across all zones in Port Susan Bay is $134.29gCm^{-2}yr^{-1}$. Carbon accumulation (gC m^{-2} yr^{-1}) is highest at the low marsh sites in Zone 4 followed by R2 in Zone 2 and the high marsh in Zone 4 ($310gCm^{-2}yr^{-1}\pm37$, $288gCm^{-2}yr^{-1}$, $252gCm^{-2}yr^{-1}\pm12$ respectively, Figure 31 and Table 5). Low rates of carbon accumulation are found at SET 5 (mud) and in the low marsh of Zone 5 ($6gCm^{-2}yr^{-1}$ and $15gCm^{-2}yr^{-1}\pm3.6$ respectively, Figure 31 and Table 5). The average carbon accumulation rate in Zone 2 (restored area) is much higher than the average across all zones ($206gCm^{-2}yr^{-1}$ versus $115gCm^{-2}yr^{-1}$). Within Zone 2, the SETs in the middle of the restored area (25 and 26) which align with sites RM1 and RM2 have higher carbon accumulation rates than RS1 and RS2 (Figure 32). RM1 has over double the carbon accumulation rate of RS1 ($289gCm^{-2}yr^{-1}$ versus $128gCm^{-2}yr^{-1}$, Figure 32).
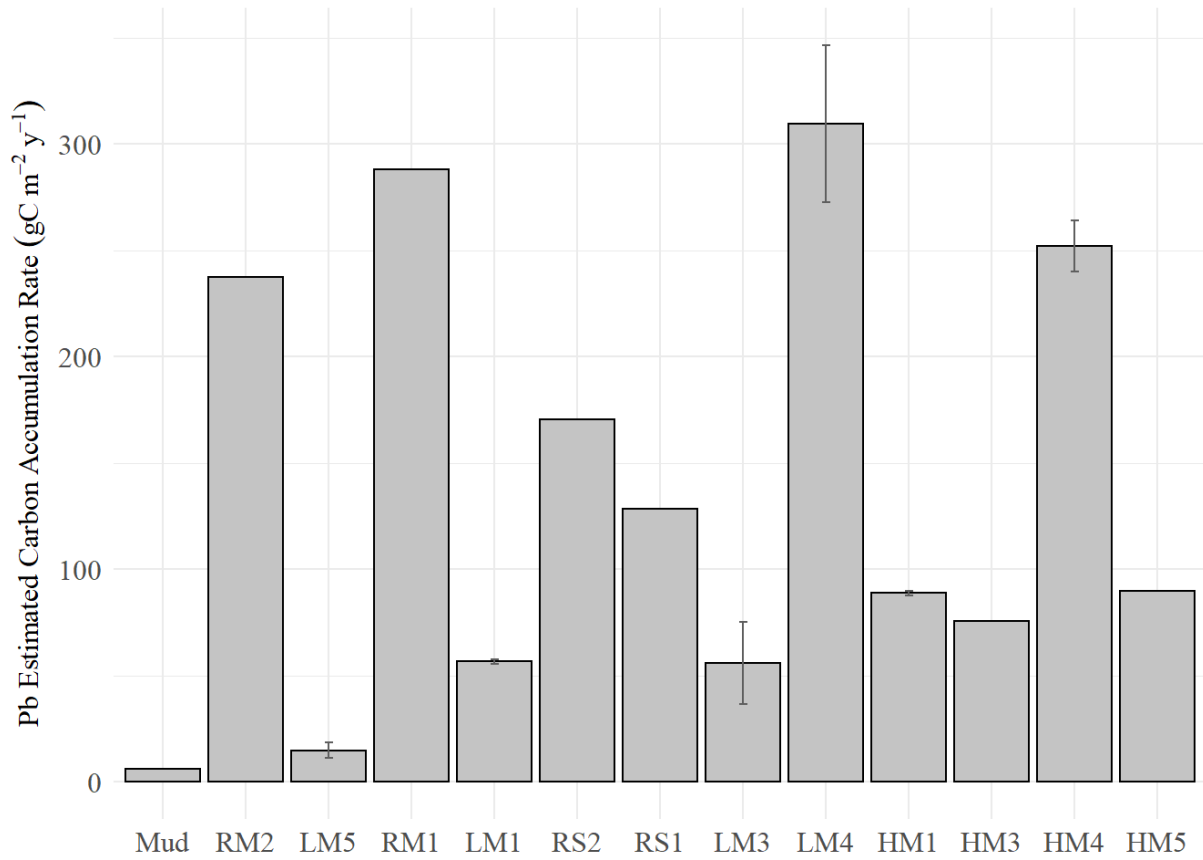
Figure 31. Estimated Pb-based carbon accumulation rate (gC m^{-2} yr^{-1}) using SET elevation change rate with standard error. Sites are arranged by increasing elevation from left to right (lowest on the left).
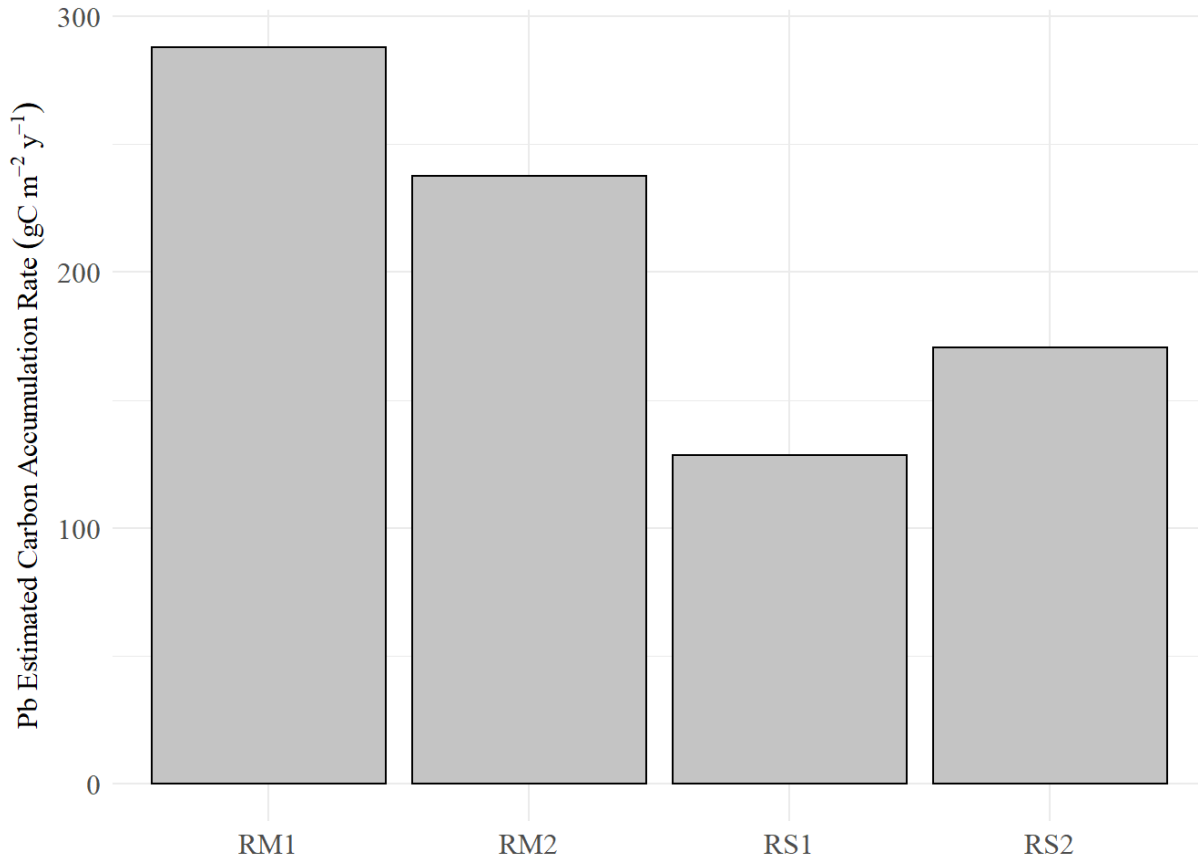
Figure 32. Estimated Pb-based carbon accumulation rate (gC m^{-2} yr^{-1}) using SET elevation change rate (Zone 2).

3.4. Discussion

3.4.1. Elevation Change Rates

Our data suggests that, aside from SET 5 in the tidal flat, the sediment elevation change in Port Susan Bay is keeping up with local relative sea level rise (RSLR). The local rate of RSLR, recorded at a nearby tide station, is 1.81 mm yr^{-1}±0.66 (NOAA, 2022). Many of the zones, such as Zone 2 (restoration area) and Zone 4, are gaining enough elevation to keep up with even intermediate and high regional RSLR future projections.

The rate of elevation change in the low marsh of Zone 4, has nearly tripled since 2018 (1.09cm yr^{-1} versus 2.72cm yr^{-1}±0.32) and the high marsh elevation change rate has slightly declined (2.46cm yr^{-1} versus 1.92cm yr^{-1}±0.09) (Poppe and Rybczyk 2021). This zone is very dynamic in

terms of hydrology and deposition (Poppe and Rybczyk 2021). Despite unreliable influx of sediment, Zone 4 has a whole has had a steady increase in elevation since 2016. Zone 5 is also dynamic, and has had years of decreased elevation (e.g. from 2017 to 2018 seen in Figure 28). The elevation change rate at the tidal flat site, as of 2020, was 0.11cm yr^{-1} which is not keeping up with local RSLR.

The average elevation change in Zone 2, the restored area, is increasing at a rate well above local RSLR (2.46cm yr^{-1}±0.42). When broken down by individual SETs, the SETs in the middle of Zone 2 (RM1 and RM2) have higher elevation change rates than those that are at the southern end (RS1 and RS2). The elevation change rates at RM2 and RS2 increased since 2018 but decreased at RM1 and RS1. It is possible that this average decrease in elevation change is part of the natural progression of this restored area.

3.4.2. Carbon Accumulation Rates

The global average salt marsh carbon accumulation rate, reported by Ouyang and Lee (2014), is 244.7gC$m^{-2}yr^{-1}$. Lower rates of carbon accumulation have been reported in nearby salt marshes, many of which were measured using ^{210}Pb dating. Crooks et al. (2014) report carbon accumulation rates ranging from 58.0gC$m^{-2}yr^{-1}$ to 352.1gC$m^{-2}yr^{-1}$ in the Snohomish estuary, Washington and Drexler et al. (2019) report rates ranging from 81gC$m^{-2}yr^{-1}$ to 224gC$m^{-2}yr^{-1}$ in the Nisqually River estuary.

Despite slight decreases in accumulation rates in the past few years, the current average carbon accumulation rate for the restoration area (Zone 2) is similar to regional estimates. RM2 and RM1, the sites in the middle of the restored area, have accumulation rates closer to the global average reported by Ouyang and Lee (2014) than RS2 and RS1 which are at the south end of the restored area near the Stillaguamish river. Data from each of the four restoration sites suggest

that Port Susan Bay is quite variable from site to site. This is likely due to spatial variation in hydrological conditions and sediment supply.

Similar to the trajectory of relative elevation change, decreasing carbon accumulation rates may be a natural part of the progression for the restored sites. The magnitude of change in the two restored sites that had lower accumulation rates than 2018 (R1 and R3) was quite large compared to the change at sites with increased rates (R2 and R4). These data are interesting because one would expect RM2 and RM1 to change in a similar direction and similarly, RS2 and RS1 because of proximity in the restored area.

As for the natural marsh sites, it is less clear why there was an overall decline in accumulation rates over the past few years. The average accumulation for the natural marsh sites is $115gCm^{-2}yr^{-1}$, much lower than the global average.

While carbon accumulation rates are higher in the restoration area than in natural marsh zones, carbon density is higher in natural marsh zones. As the restored marsh matures, carbon density may increase further increasing the carbon accumulation rate.

4. NET SOURCE OR SINK?

The restored area of Port Susan Bay, Washington is a net sink of carbon, storing 96gC m^{-2} yr^{-1} more than the greenhouse gas carbon equivalent of methane it emits. Even high emission estimates from the restored area of Port Susan Bay are outweighed by the average carbon accumulation rate (130.75gC m^{-2} yr^{-1} and 110.7gC m^{-2} yr^{-1} versus 206.04gC m^{-2} yr^{-1}, Figure 33). These results suggest that this site exhibits negative radiative forcing similar to other tidal wetlands (e.g. Arias-Ortiz et al. 2021). Estimates based on redox potential, vegetation composition, and sulfate suggest even lower emissions most of the year. The highest emission estimates, if existent, are likely at the south end of the restoration area (RS1 and RS2) during late summer. The lowest emissions are likely to occur in the winter when the sediment temperature drops.

Carbon accumulation in the restoration area (Zone 2) is 206gCm^{-2}yr^{-1} (using Pb-based estimate) which is comparable to nearby estuaries. This accumulation rate may decrease over time as part of the natural progression at the site. The average carbon accumulation throughout the natural marsh sites is nearly half that of the restoration site (115gCm^{-2}yr^{-1}). These estimates are important for assessing the carbon budget of this site. If the accumulation rate outweighs the emissions, this site is a good candidate for carbon credits. Methane emission estimate methods using salinity as a sole proxy to estimate emissions represent a ceiling for the maximum predicted fluxes for this site (IPCC 2013: 19.37gCH4 m^{-2} yr^{-1} and Poffenbarger et al. 2011: 16.4gCH4 m^{-2} yr^{-1}). While these represent high estimates, other indicators which hare associated with the conditions for methanogenesis, such has redox potential indicate negligible emissions. This is an important step in completing the greenhouse gas budget for this site and to determine the viability for assigning carbon credits to a project like this. The methane measurement

methods customized for this project, with effective instrumentation, proves to be a cost-effective way to assess emissions in the field. Despite the limitations of this project, the information collected will contribute to a growing repository of post-restoration data and inform future projects.
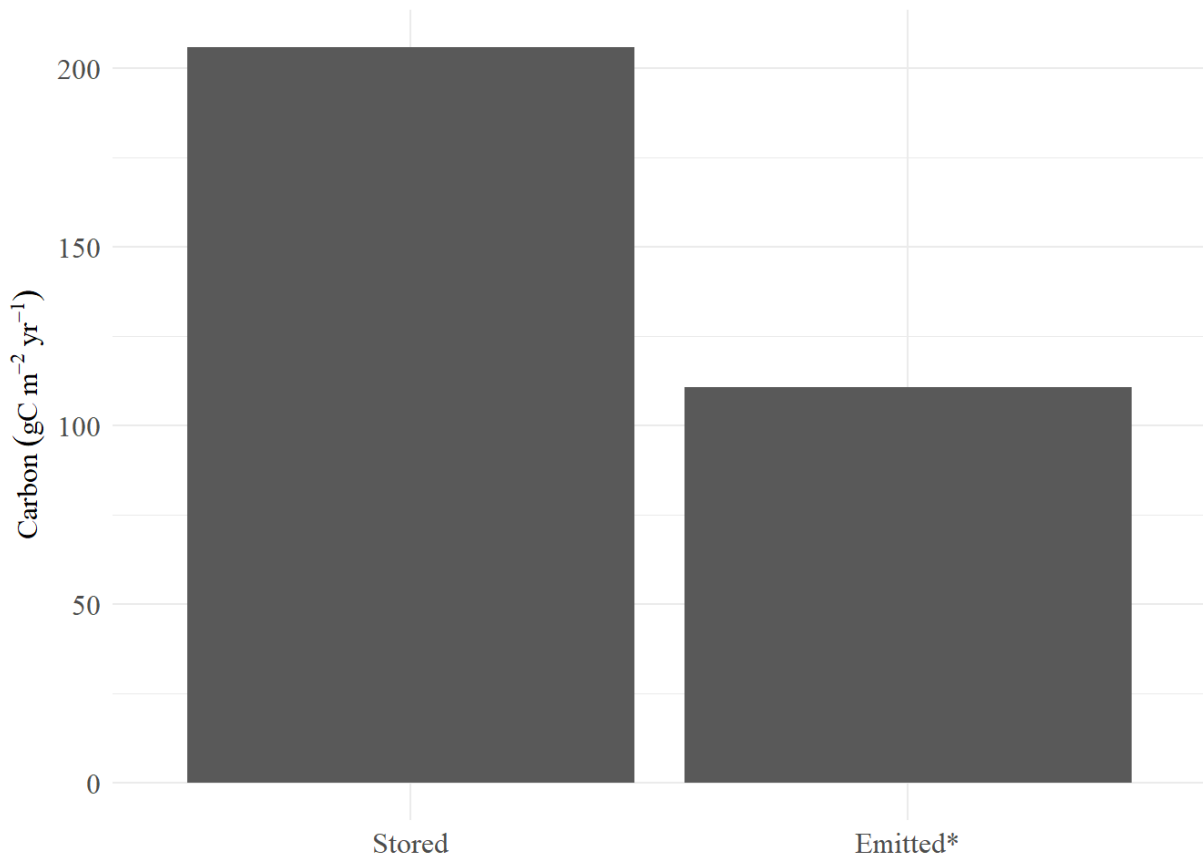

Figure 33. Carbon accumulation (stored) in Port Susan Bay, WA from 2021 SET measurements. Estimated carbon emission rate based on published methane data by *Poffenbarger et al. (2011). Methane emissions converted to carbon dioxide equivalent and carbon emission using ratio of 0.27.

5. WORKS CITED

Al-Haj, A. N. and R. W. Fulweiler. 2019. A synthesis of methane emissions from shallow vegetated coastal ecosystems. Global Change Biology 26:2988-3005.

Arias-Ortiz, A., P. Y. Oikawa, J. Carlin, P. Masque, J. Shanhan, S. Kanneg, A. Paytan and D. D. Baldocchi. 2021. Tidal and Nontidal Marsh Restoration: A Trade-Off Between Carbon Sequestration, Methane Emissions, and Soil Accretion. Journal of Geophysical Research: Biogeosciences, 126.

Batker, D., P. Swedeen, R. Costanza, I. de la Torre, R.M. Boumans, and K. Bagstad. 2008. A new view of the Puget Sound economy: the economic value of nature's services in the Puget Sound Basin. Report by Earth Economics, Tacoma, WA.

Billett, M. F. and T. R. Moore. 2008. Supersaturation and evasion of CO_2 and CH_4 in surface waters at Mer Bleue peatland, Canada. Hydrological Processes 22:2044-2054.

Bridgham, S. D., H. Cadillo-Quiroz, J. K. Keller, and Q. Zhuang. 2013. Methane emissions from wetlands: biogeochemical, microbial, and modeling perspectives from local to global scales. Global Change Biology 19:1325-1346.

Bhullar, G. S., M. Iravani, P. J. Edwards and H. Olde Venterink. 2013. Methane transport and emissions from soil as affected by water table and vascular plants. BMC Ecology 13:32.

Christensen, T.R., A. Ekberg, L. Strom, M. Mastepanov, N. Panikov, M. Oquist, B.H. Svensson, H. Nykanen, P.J. Martikainen, and H. Oskarsson. 2003. Factors controlling large scale variations in methane emissions from wetlands. Geophysical Research Letters 30(7):1414. doi:10.1029/2002GL016848

Cahoon, D. 2022. The Surface Elevation Table and Marker Horizon Technique. Available online at: https://www.usgs.gov/centers/eesc/science/surface-elevation-table (Accessed 14 April 2022).

Callaway, J.C., E.L. Borgnis, R.E. Turner, and C.S. Milan. 2012. Carbon sequestration and sediment accretion in San Francisco tidal wetlands. Estuaries and Coasts 35:1163-1181.

CLEAR Center 2019. What is Carbon Sequestration and How Does it Work? Available online at: https://clear.ucdavis.edu/explainers/what-carbon-sequestration#:~:text=Carbon%20is%20sequestered%20in%20soil,also%20store%20carbon%20as%20carbonates (Accessed 14 April 2022)

Crooks, S., J. Rybczyk, K. O'Connell, D. L. Devier, K. Poppe, and S. Emmett-Mattox. 2014. Coastal blue carbon opportunity assessment for the Snohomish Estuary; the climate benefits of estuary restoration. Report by Environmental Science Associates, Western Washington University, EarthCorps, and Restore America's Estuaries.

de Angelis, M. A., and M. D. Lilley. 1987. Methane in surface waters of Oregon estuaries and rivers. Limnology and Oceanography 32:716-722.

Dean, J. F., J. J. Middleburg, T. Röckmann, R. Aerts, L. G. Blauw, M. Egger, M. S. M. Jetten, A. E. E. de Jong, O. H. Meisel, O. Rasigraf, C. P. Slomp, M. G. in't Zandt, and A. J.

Dolman. 2018. Methane feedbacks to the global climate system in a warmer world. Reviews of Geophysics 56:207-250.

Derby, R. K., B. A. Needleman, A. A. Roden, and J. P. Megonigal. 2021. Vegetation and hydrology stratification as proxies to estimate methane emission from tidal marshes. Biogeochemistry.

Drexler, J. Z., I. Woo, C. C. Fuller and G. Nakai. 2019. Carbon accumulation and vertical accretion in a restored versus historic salt marsh in southern Puget Sound, Washington, United States. Restoration Ecology 27:1117-1127.

Environmental Protection Agency. 2017. Understanding global warming potentials. Available online at https://www.epa.gov/ghgemissions/understanding-global-warming-potentials (Accessed 17 October 2019).

Environmental Protection Agency. 2021. Understanding Global Warming Potentials. Available online at: https://www.epa.gov/ghgemissions/understanding-global-warming-potentials (Accessed 14 April 2022).

Eurofins. 2016. Recommended Containers, Preservation, Storage, & Holding Times. Available online at: https://www.eurofinsus.com/media/447768/appendix-d-section-5-attachment-holdtime-container-list_2016-july.pdf (Accessed 14 April 2022).

Fuller, R. N. 2018. Port Susan Bay Restoration Project: Final Monitoring Report. Report prepared for The Nature Conservancy: (in press).

Gunn, C. 2016. Methane emissions along a salinity gradient of a restored salt marsh in Casco Bay, Maine. M.S. Thesis. Bates College, Lewiston, Maine.

Harley, J. F., L. Carvalho, B. Dudley, K. V. Heal, R. M. Rees, and U. Skiba. 2015. Spatial and seasonal fluxes of the greenhouse gases N2O, CO2, and CH4 in a UK macrotidal estuary. NERC Open Research Archive and Centre for Ecology and Hydrology.

Harris, D. C. 2010. Quantitative Chemical Analysis Eighth Edition. W. H. Freeman and Company. New York, NY.

Holm, G.O., B.C. Perez, D.E. McWhorter, K.W. Krauss, D.J. Johnson, R.C. Raynie, and C.J. Killebrew. 2016. Ecosystem level methane fluxes from tidal freshwater and brackish marshes of the Mississippi River Delta: implications for coastal wetland carbon projects. Wetlands 36:401-413.

Howes, B. L. J. W. Dacey and S. G. Wakeham. 1985. Effects of sampling technique on measurements of porewater constituents in salt marsh sediments. Limnology and Oceanography 30:221-227.

Hu, M., B. J. Wilson, Z. Sun, P. Ren, and C. Tong. 2016. Effects of the addition of nitrogen and sulfate on CH4 and CO2 emissions, soil, and pore water chemistry in a high marsh of the Min River estuary in southeastern China. Science of the Total Environment 579:292-304.

IPCC. 2013. 2013 Supplement to the 2006 IPCC Guidelines for National Greenhouse Gas Inventories: Wetlands. Available online at: https://www.ipcc.ch/publication/2013-

supplement-to-the-2006-ipcc-guidelines-for-national-greenhouse-gas-inventories-wetlands/ (Accessed 14 April 2022).

Janousek, C. S. Bailey, S. van de Wetering, L. Brophy, S. Bridgham, M. Schultz and M. Tice-Lewis. Early post-restoration recovery of tidal wetland structure and function at the Southern Flow Corridor project, Tillamook Bay, Oregon. Oregon State University, Tillamook Estuaries Partnership, Confederated Tribes of Siletz Indians, Institute for Applied Ecology, and University of Oregon.

Kahmark, K., N. Millar and G. P. Robertson. 2020. Static Chamber Method for Measuring Soil Greenhouse Gas Fluxes. W.K. Kellogg Biological Station, Michigan State University.

Kao-Kniffin, J., D. S. Freyre and T. S. Balser. 2010. Methane dynamics across wetland plant species. Aquatic Botany 93:107-113.

Keller, J. K. 2019. In L. M. Windham-Myers, S. Crooks, and T. G. Roxler (editors). A Blue Carbon Primer, CRC Press, Boca Raton, FL. Pp. 93-106.

Lane, R. R., S. K. Mack, J. W. Day, R. Kempka, and L. J. Brady. 2017. Carbon sequestration in a forested wetland receiving treated municipal effluent. Wetlands 37:861-873.

Lannbroek, H. J. 2009. Methane emission from natural wetlands: interplay between emergent macrophytes and soil microbial processes. A mini-review. Annals of Botany 105:141-153.

Looman, A., I. R. Santos, D. R. Tait, J. Webb, C. Holloway, and D. T. Maher. 2019. Dissolved carbon, greenhouse gases, and Ȯ13C dynamics in four estuaries across a land use gradient. Aquatic Sciences 81:22.

Lynch, J. C., P. Hensel and D. R. Cahoon. 2015. The Surface Elevation Table and Marker Horizon Technique. Natural Resource Report NPS/NCBN/NRR 2015/1078. National Park Service, Fort Collins, Colorado.

Mitsch, W. J., and J. G. Gosselink. 2015. Wetlands. John Wiley & Sons, Hoboken, NJ.

McLeod, E., G. L. Chmura, S. Bouillon, R. Salm, M. Bjork, C. M. Duarte, C. E. Lovelock, W. H. Schlesinger, and B. R. Silliman. 2011. A blueprint for blue carbon: toward an improved understanding of the role of vegetated coastal habitats in sequestering CO2. Frontiers in Ecology and the Environment 9:552-560.

Murray, B. C., L. Pendleton, W. A. Jenkins, and S. Sifleet. 2011. Green payments for blue carbon economic incentives for protecting threatened coastal habitats. Duke Nicholas Institute for Environmental Policy Solutions.

Muller, P., T. J. Mozder, J. A. Langley, L. R. Aokij, G. L. Noyce and J. P. Megonigal. 2020. Plant species determine tidal wetland methane response to sea level rise. Nature Communications 11:5154.

Morgan, E. and D. Siemann. 2011. Summary of climate change effects on major habitat types in Washington state marine and coastal habitats. Washington Department of Fish and Wildlife and the National Wildlife Federation. Available online at

https://wdfw.wa.gov/sites/default/files/publications/01239/wdfw01239.pdf (Accessed 17 October 2019).

NOAA Tides and Currents. 2022. National Oceanic and Atmospheric Administration. Available online at: https://tidesandcurrents.noaa.gov/noaatidepredictions.html?id=9448094 (Accessed 15 April 2022).

NOAA 2022. What is Blue Carbon? Available online at: https://oceanservice.noaa.gov/facts/bluecarbon.html (Accessed 14 April 2022).

National Oceanic and Atmospheric Administration. 2017. Monitoring Estuaries. Available online at https://oceanservice.noaa.gov/education/kits/estuaries/estuaries10_monitoring.html (Accessed 17 October 2019).

Neubauer, S. C. 2021. Global warming potential is not an ecosystem property. 2021. Ecosystems.

Neubauer, S. C., K. Gilver, S. K. Valentine and J. P. Megonigal. 2005. Seasonal patterns and plant-mediated controls of subsurface wetland biogeochemistry. Ecology 86:3334-3344.

Ouyang, X. and S. Y. Lee. 2014. Updated estimates of carbon accumulation rates in coastal marsh sediments. Biogeosciences 11:5057-5071.

Poffenbarger, H. J., B. A. Needelman, and J. P. Megonigal. 2011. Salinity Influence on Methane Emissions from Tidal Marshes. Society of Wetland Scientists 31:831-842.

Poppe, K. L. 2015. An ecogeomorphic model to assess the response of Padilla Bay's eelgrass habitat to sea level rise. M.S. Thesis. Western Washington University, Bellingham, Washington.

Poppe, K. and J. Rybczyk. 2019. A blue carbon assessment for the Stillaguamish River estuary: Quantifying the climate benefits of tidal marsh restoration. Western Washington University, Bellingham.

Poppe, K. L and J. M. Rybczyk. 2021. Tidal marsh restoration enhances sediment accretion and carbon accumulation in the Stillaguamish River estuary, Washington. PLoS ONE 16.

R Version 4.1.2

Schultz, M. 2019. The effect of land use on greenhouse gas emission along salinity gradients in Pacific Northwest coastal wetlands. M.S. Thesis, University of Oregon, Eugene, Oregon.

The Nature Conservancy. 2021. Port Susan Bay. Available online at https://www.washingtonnature.org/port-susan-bay (Accessed 8 March 2022).

The Nature Conservancy. 2015. Port Susan Bay Estuary Restoration Project – Post Construction Monitoring. Port Susan Bay Estuary Restoration Monitoring Progress Report, December 2015: (in press).

Vizza, C., W. E. West, S. E. Jones, J. A. Hart and G. A. Lamberti. 2017. Regulators of coastal wetland methane production and responses to simulated global change. Biogeosciences 14:431-446.

VCS (Verified Carbon Standard). 2015. VM0033 Methodology for Tidal Wetland and Seagrass Restoration, v1.0. Authors: Emmer, I., B. Needelman, S. Emmett-Mattox, S. Crooks, P. Megonigal, D. Myers, M. Oreska, K. McGlathery, and D. Shoch. Developed by Restore America's Estuaries and Silvestrum. Verified Carbon Standard, Washington, DC.

VCS (Verified Carbon Standard). 2021. Program Definitions v4.1.

VCS (Verified Carbon Standard). 2014. VM0024 Methodology for Coastal Wetland Creation, v1.0. Louisiana Coastal Protection and Restoration Authority, CH2M Hill, and EcoPartners.

Wang, Z. P., R. D. DeLuane, P. H. Masscheleyn and W. H. Patrick, Jr. 1993. Soil redox and pH effects on methane production in a flooded rice soil. Soil Society of American Journal 57:382-385.

Whalen, S. C. 2005. Biogeochemistry of methane exchange between natural wetlands and the atmosphere. Environmental Engineering Science 22:73-94.

6. Appendix A: Methane Flux Field Methods

6.1. Introduction

Methane was measured using the static chamber (Figure 34) and headspace sampling method with subsequent analysis on a gas chromatography flame ionization detector (GC-FID). These methods are similar to studies done by Lane et al. (2017), Poffenbarger et al. (2011), Billet and Moore (2008), and Gunn (2016).

The total budget for these methods in Port Susan Bay, WA was approximately $2,500 (see Appendix G for itemized budget). These methods provide a cost-effective way to assess emissions with limited supplies.

Figure 34. Static chamber in Port Susan Bay

6.2. Methods

6.2.1. Chamber Design and Creation

Static gas chambers were modeled off studies done by Cailene Gunn (2016) and Kahmark, et al. (2020). The chambers were built by James Mullen and Vincent Hill in the Bond Hall Shop at Western Washington University.

The chamber body (Figure 35.a.) was made of 20.32cm diameter white polyvinyl chloride (PVC) pipes (standard dimension ratio 26). Chambers were initially slightly taller than one meter to accommodate tall vegetation. After preliminary deployments, the chambers were cut down to 67cm for most of the project. Chamber height was determined by balancing maximizing sediment surface area to chamber volume with allowing clearance for tall, dense vegetation. A hole was drilled in the center of the chamber body and fitted with Chemglass sleeve-type septum stopper sealed with silicon glue. This septum served as the port for sample collection. One end of the chamber body was sharpened for insertion into sediment.

The lid was made of double-layer, clear plexiglass with a foam seal to sit on the rim of the chamber body. A metal eye bolt was drilled into the middle of the lid to hold a temperature logger and fan. This bolt was held in place with metal washers. I used a thin PVC pipe to hold the Onset HOBO pendant temperature logger and O2 Cool fan in the interior middle of the chamber (Figure 35.b.). The fan was used to circulate air in the chamber to create a representative air sample during collection. The HOBO logger recorded chamber temperature.

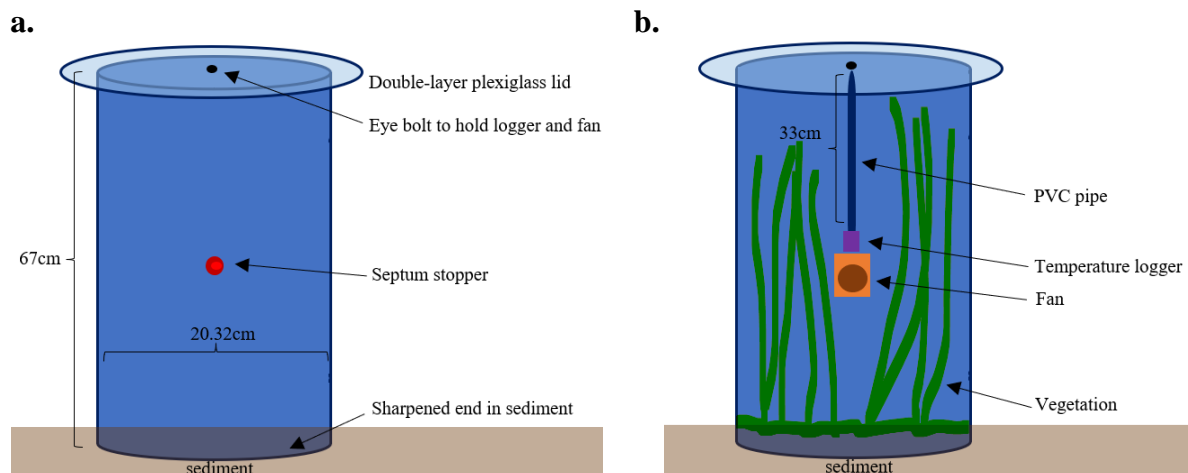Three chambers were made for simultaneous triplicate measurements at each site.

Figure 35. Static chamber exterior (a) and static chamber interior (b)

6.2.2. Field Methods

Immediately after arriving to each site, all three chambers (sharpened-side-down) were placed on the sediment so they could settle and create a seal. The chambers were left on the sediment surface for 60 to 90 minutes. I withdrew air samples at 15-minute increments starting at T0 which served as a baseline. I waited 30 minutes before T1 samples during 90-minute deployments. A wooden bench was used to minimize sediment disturbance and ebullition near the chambers during sampling (Figure 36.a.).

Immediately before the first measurement (T0), the fan was turned on and the lid was secured on top of the chamber body. 30ml (BD slip-tip) or 60ml (BD Luer-Lok) plastic syringe fitted with a 22-gauge hypodermic needle was used to withdraw the gas samples out of the chambers. The needle was flushed in the chamber three times and before withdrawing approximately 30ml of gas, through the septum (Figure 36.b.). To minimize mixing with atmospheric air, the syringe was depressed to continuously flush the needle before immediately injecting 12ml of the sample into pre-evacuated LabCo exetainer vials. I repeated this at each replicate site at 15-minute

increments throughout the deployment time (see Table 6 for timetable). I measured each replicate site simultaneously, leaving approximately two minutes between each replicate chamber measurement. Three atmospheric samples were taken at the main site to rectify the baseline (T0) measurements.

The vials were stored in a cool dark place and analyzed on the GC-FID within 30 days of sampling.

Field sampling took place at low tide every month during the Spring and Summer and once in the Fall and Winter (table 7).

a.   b.

Figure 36. Static chamber in tall vegetation with bench set-up (a) Static chamber gas sample collection through septum (b)

Table 6. Example timetable for sample collection

Time (min)	Sample Number
0:00	Chamber 1 T_0CH_4 sample
0:02	Chamber 2 T_0CH_4 sample
0:04	Chamber 3 T_0CH_4 sample
0:30	Chamber 1 T_1CH_4 sample
0:32	Chamber 2 T_1CH_4 sample
0:34	Chamber 3 T_1CH_4 sample
0:45	Chamber 1 T_2CH_4 sample
0:47	Chamber 2 T_2CH_4 sample
0:49	Chamber 3 T_2CH_4 sample
1:00	Chamber 1 T_3CH_4 sample
1:02	Chamber 2 T_3CH_4 sample
1:04	Chamber 3 T_3CH_4 sample
1:15	Chamber 1 T_4CH_4 sample
1:17	Chamber 2 T_4CH_4 sample
1:19	Chamber 3 T_4CH_4 sample
1:30	Chamber 1 T_5CH_4 sample
1:32	Chamber 2 T_5CH_4 sample
1:34	Chamber 3 T_5CH_4 sample

Table 7. Field measurement schedule

Month and Year	Date
August 2020	RS1: 8/28, RS2: 8/29, RM1 and RM2: 8/30
October 2020	RS1 and RS2: 10/11, RM1 and RM2: 10/12
February 2021	RS1 and RS2: 2/9, RM1 and RM2: 2/8
May 2021	RS1 and RS2: 5/25, RM1 and RM2: 5/26
June 2021	RS1 and RS2: 6/23, RM1 and RM2: 6/22
July 2021	RS1 and RS2: 7/22, RM1 and RM2: 7/21
August 2021	RS1 and RS2: 8/20, RM1 and RM2: 8/19
September 2021	RM2: 9/19

6.2.3. Laboratory Methods

I used an Agilent 6890 Plus gas chromatograph with a flame ionization detector (GC-FID) to

analyze my gas samples. The GC-FID was fitted with a two-meter SilcoSmooth stainless steel

Restek micropacked ShinCarbon ST column (Figure 37.a.) and helium was used as the carrier

gas. This column works well for small hydrocarbons. We used GC-FID settings as described by

Gunn (2016). The retention time for methane was approximately four minutes and the total run time was ten minutes for each sample.

I manually injected samples using a Hamilton gastight 250uL syringe through a 11mm Agilent inlet septa. Sample injections were always 250uL. I withdrew slightly more than 250uL of the sample to flush the needle while transporting it from the exetainer vial to the instrument. Peak area integrations of the chromatographs were also done manually using ChemStation (Figure 37.b.). I ran standard curves using various volumes of 100ppm methane in nitrogen. Blank exetainers were used as the zero measurements to account for exetainer noise in the samples.

We used Origin software to perform a baseline correction to each chromatograph to account for drift. After correcting for this drift, the standard curve can be applied to the sample peak areas to calculate methane content in each sample.

GC-FID instrument signal detection limit, minimum detectable concentration, and lower limit of quantitation were calculated using equations described in Quantitative Chemical Analysis Eight Edition (Harris, 2010).

a.

b.
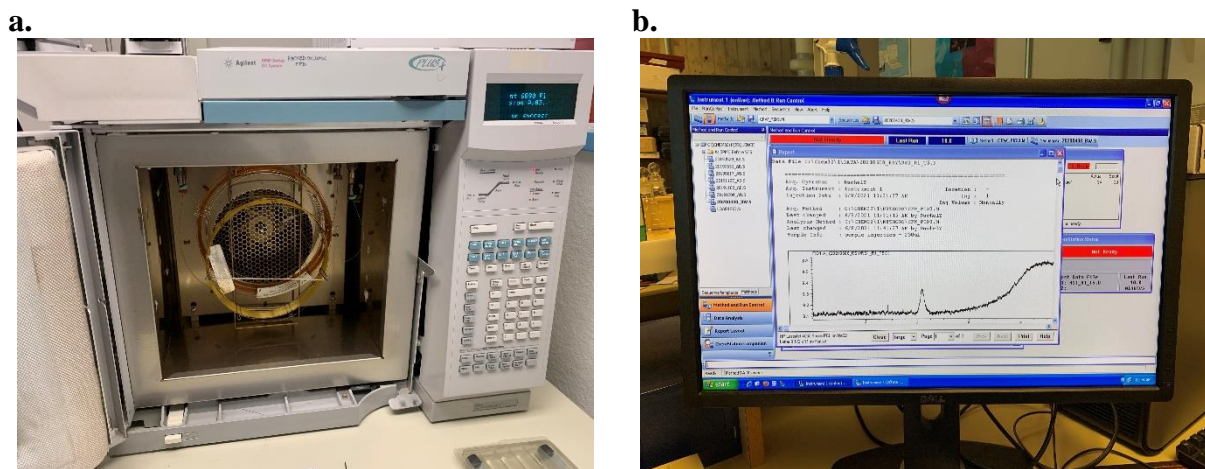
Figure 37. GC-FID Restek column (a) and GC-FID chromatograph in ChemStation (b)

6.2.4. Methane Flux Calculations

Methane (CH_4) flux is commonly reported in $gCH_4 \, m^{-2} \, yr^{-1}$. Flux is calculated using the sample peak areas from the GC-FID chromatograph, volumetric standard curve, injection volume, chamber volume, and chamber footprint using the following workflow.

6.2.4.1. Methane Flux Calculation from Volumetric Standard Curve

First, convert standard curve units (μL of 100ppm CH_4) to $\mu mol \, CH_4$ (Equation 4). This accounts for the varying volumes of 100ppm CH_4 and the molar mass of CH_4. Parts per million is represented by $mg \, L^{-1}$.

$$\underline{\qquad} \mu L \times \frac{100mg}{L} \times \frac{1g}{1000mg} \times \frac{1mol}{16.04g} \times \frac{1L}{1e^6 \mu L} \times \frac{1e^6 \mu mol}{1mol} = \underline{\qquad} \mu mol \, CH_4$$

Equation (4)

Plot the standard curve in $\mu mol \, CH_4$ (example in Figure 37).
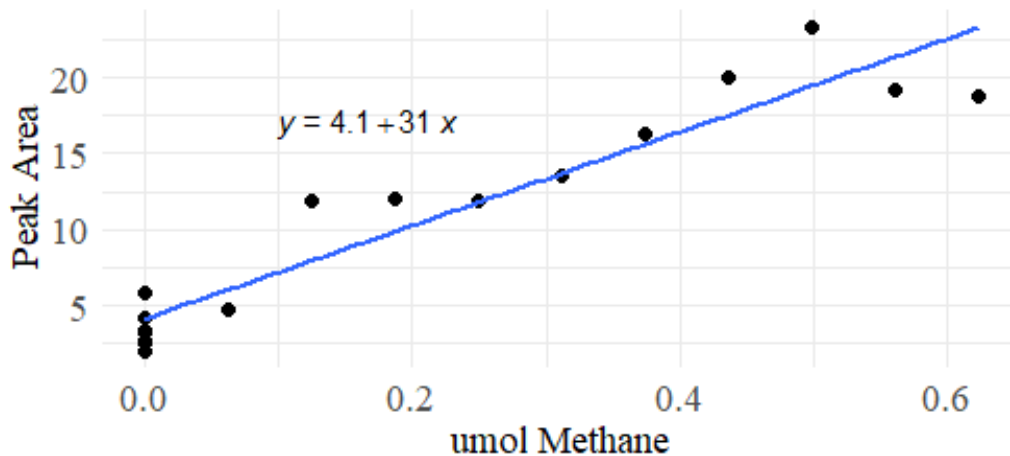
Figure 37. Methane standard curve

Apply the standard curve equation to each sample peak area to calculate $\mu mol \, CH_4$ in each sample (solve for x). Use Equation 5 to account for the sample injection volume (250μL) of each sample to get μmol per μL.

$$\frac{\mu mol}{} \times \frac{1}{250\mu L} = \frac{\mu mol\ CH_4}{\mu L}$$

Equation (5)

Multiply the amount of CH$_4$ (in µmol) per µL in each sample by the chamber volume to

determine the amount (µmol) of methane in the chamber (volume in µL) using Equation 6.

The chamber volume should be representative of only the volume above the sediment (i.e.

subtract volume inserted into sediment).

$$\frac{\mu mol\ CH_4}{\mu L} \times \frac{\mu L}{} = \_\_\_\mu mol\ CH_4$$

Equation (6)

To determine the rate of methane emission for each chamber, plot the sample µmol CH$_4$ over

time (min). The slope of the linear regression will be in µmol CH$_4$ min^{-1} (simplified example in

Figure 38).
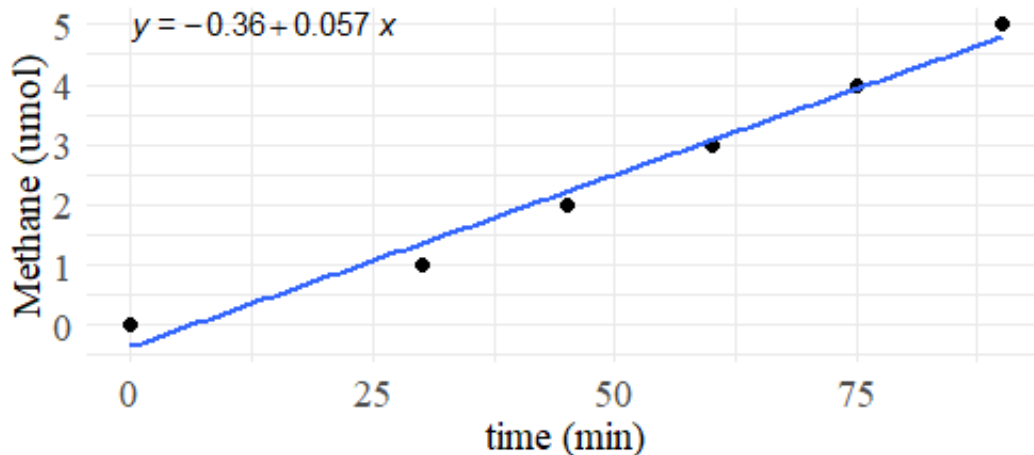
Figure 38. Example rate of methane emission plot

Use the rate of methane emission (in µmol CH$_4$ min^{-1}) and the chamber footprint to calculate

methane flux (µmol CH$_4$ m^{-2} min^{-1}). Equation 7 uses 0.2032m to calculate the chamber footprint

(20.32cm diameter).

$$\frac{\mu mol}{min} \times \frac{1}{\pi(\frac{0.2032m}{2})^2} = \frac{\mu mol\ CH_4}{min\ m^2}$$

Equation (7)

Finally, Equation 8 provides the unit conversions needed to get methane flux in commonly

reported units ($gCH_4\ m^{-2}\ yr^{-1}$).

$$\frac{\mu mol}{min\ m^2} \times \frac{16.04g}{mol} \times \frac{1mol}{1e^6umol} \times \frac{525600min}{yr} = \frac{g\ CH_4}{m^2\ yr}$$

Equation (8)

6.2.4.2. Methane Flux Conversion to Carbon Dioxide Equivalent

The flux calculated in section 2.4.2.1. can be converted to a carbon equivalent using Equation

9. Equation 9 assumes the global warming potential of methane as 25 times that of carbon

dioxide. The global warming potential and conversion factor is based on the

Intergovernmental Panel on Climate Change (IPCC) AR4 report. This converted metric can

now be used in the carbon budget to assess carbon emissions.

$$\frac{g\ CH_4}{m^2\ yr} \times \frac{25(GWP)}{} \times \frac{12g}{44g} = \frac{gC}{m^2\ yr}$$

Equation (9)

6.3. Limitations to Methane Flux Measurements in Port Susan Bay

My methane quantification was not successful for this project because the Agilent 6890 GC-FID

was not sensitive enough for samples collected at Port Susan Bay. If it had been successful, I

could have calculated flux using the volumetric standard curve (laid out above) or by using a

concentration standard curve. Once a flux is calculated from the standard curve, the carbon

dioxide equivalent can be compared against carbon stocks and accumulation to determine if the

system is a net source or sink.

7. Appendix B: Geographic Coordinates of SETs in Port Susan Bay, Washington

Table 8. SET geographic coordinates and ID in Port Susan Bay, WA.

Marsh Zone	Marsh Elevation	Latitude	Longitude	ID
5	High	48.227	-122.384	Z5 S1 HE
5	High	48.227	-122.383	Z5 S2 HE
5	Low	48.226	-122.383	Z5 S3 LE
5	Low	48.226	-122.383	Z5 S4 LE
4	High	48.217	-122.37	Z4 S21 HE
4	High	48.217	-122.37	Z4 S22 HE
4	Low	48.216	-122.370	Z4 S23 LE
4	Low	48.216	-122.37	Z4 S24 LE
6	Low	48.202	-122.386	ZMud S5 UT
2	High	48.204	-122.37	Z2 S25 RET
2	High	48.202	-122.367	Z2 S26 RET
2	High	48.199	-122.365	Z2 S27 RET
2	High	48.198	-122.365	Z2 S28 RET
3	Low	48.201	-122.373	Z3 S13 LE
3	High	48.201	-122.372	Z3 S11 HE
3	High	48.200	-122.371	Z3 S20 HE
3	Low	48.201	-122.373	Z3 S16 LE
1	High	48.192	-122.363	Z1 S7 HE
1	High	48.191	-122.363	Z1 S8 HE
1	Low	48.188	-122.363	Z1 S9 LE
1	Low	48.187	-122.363	Z1 S10 LE

8. Appendix C: Summary of VCS Methodologies

Table 9. Methods for methane emission estimation

Estimation Method	Methane Emission Estimate	Source
Proxy	$GHG_{WPS\text{-}soil\text{-}CH4,i,t} = f(\text{GHG emission proxy}) \times CH_4\text{-}GWP$ (unit: CH_4 emissions from SOC pool in project scenario in $tCO_2e\ ha^{-1}yr^{-1}$)	VCS 2013
IPCC Emission Factors	$CH_{4\text{-}SO\text{-}REWET} = \sum_v (A_{REWET} \times EF_{REWET})_v$ Where: A_{REWET}=area of rewetted soil in ha (by vegetation type) EF_{REWET}=CH_4 emissions from soils; if salinity <18ppt: $193.7 kgCH_4 ha^{-1}yr^{-1}$ and if salinity >18ppt: $0 kgCH_4 ha^{-1}yr^{-1}$ (unit: $kgCH_4 yr^{-1}$, by vegetation type)	IPCC 2013 Guidelines
Published Values	Salinity < 0.5ppt: $41.9 gCH_4 m^{-2}yr^{-1}$ ($10.5 MgCO_2\ ha^{-1}\ yr^{-1}$) Salinity 0.5-5ppt: $150\ gCH_4 m^{-2}yr^{-1}$ ($37.5 MgCO_2\ ha^{-1}\ yr^{-1}$) Salinity 5-18ppt: $16.4\ gCH_4 m^{-2}yr^{-1}$ ($4.1 MgCO_2\ ha^{-1}\ yr^{-1}$) Salinity >18ppt: $1.12\ gCH_4 m^{-2}yr^{-1}$ ($0.3 MgCO_2\ ha^{-1}\ yr^{-1}$)	Poffenbarger et al. 2011
Default Factors	Salinity >18ppt: $GHG_{WPS\text{-}soil\text{-}CH4,i,t} = 0.011 tCH_4 ha^{-1}yr^{-1} \times CH_4\text{-}GWP$ Salinity ≥ 20ppt: $GHG_{WPS\text{-}soil\text{-}CH4,i,t} = 0.0056 tCH_4 ha^{-1}yr^{-1} \times CH_4\text{-}GWP$	VCS 2013

9. Appendix D: Correlation Coefficients for all Proxy Variables
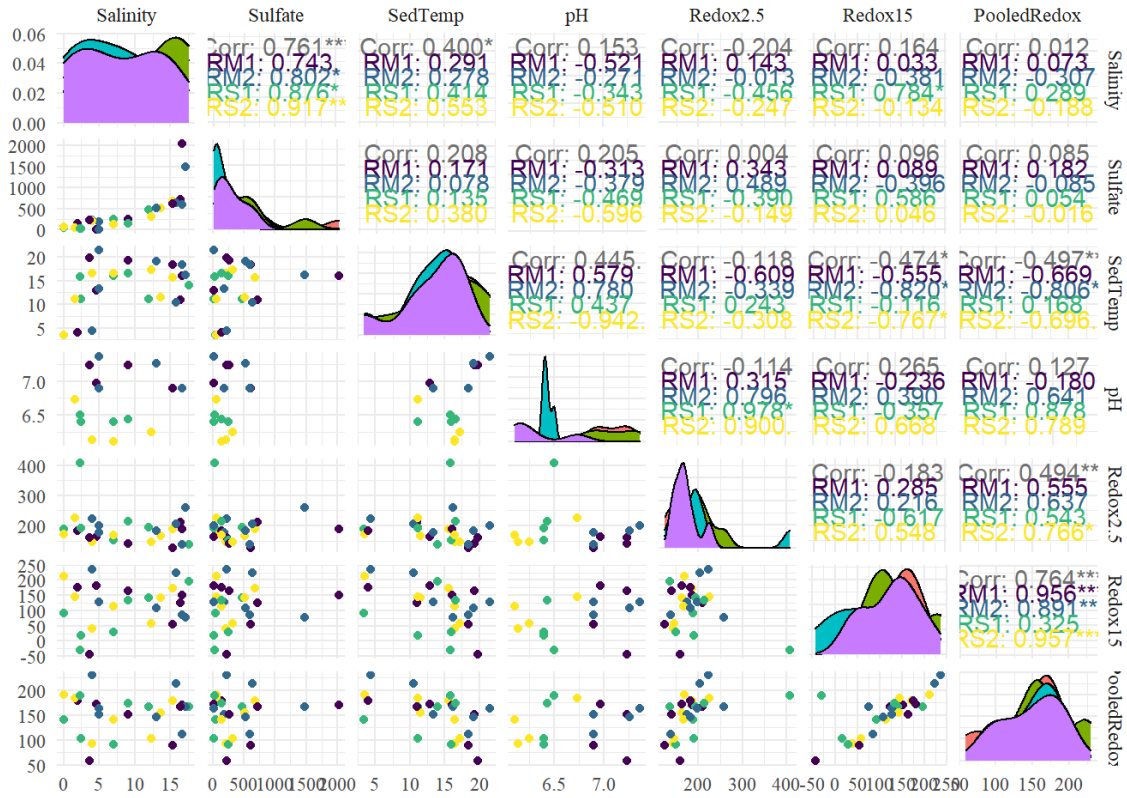
Figure 39. Correlation coefficients (r) for all variables (salinity, sulfate, sediment temperature, pH, and redox) separated out for each site (RM1, RM2, RS1, and RS2) and pooled for each site. Correlations were done using the Spearman method to account for non-normal data. Scatter plots of each variable are depicted in the lower left and individual correlation coefficients are displayed in the upper right.

10. Appendix E: Summary of Redox Electrodes Used in Field

Table 10. Number of redox electrodes and equilibration time used during each sampling period

Date	Number of electrodes	Equilibration time
August 2020, October 2020	4 at each depth	90 minutes at each depth
February 2021	16 at 2.5cm and 8 at 15cm	45 minutes at each depth
May 2021, June 2021, July 2021, August 2021, September 2021	3 electrodes measured twice at each depth	2-3 minutes at each depth

11. Appendix F: Multi-dimensional Scaling Results
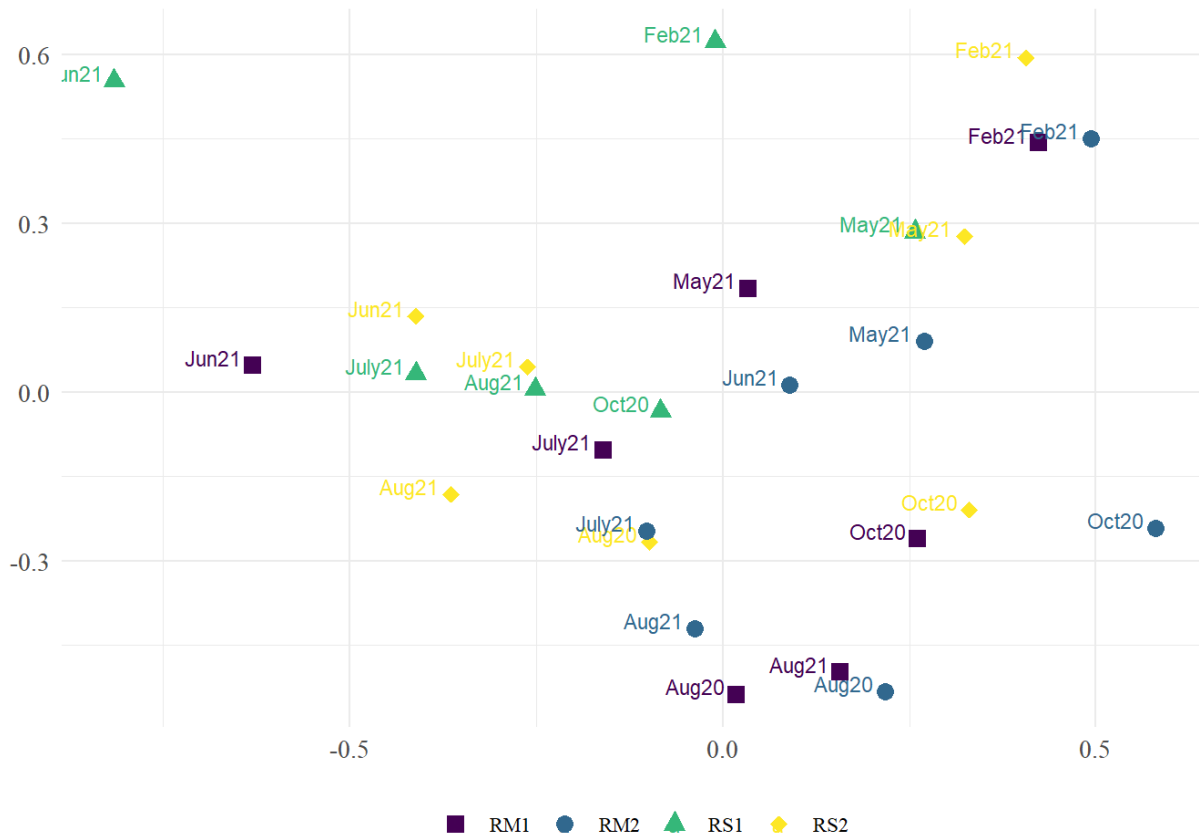
Figure 40. Multi-dimensional scaling (MDS) plot using several variables (salinity, sulfate, sediment temperature, pH, and redox) to map out site similarities over time (RM1, RM2, RS1, and RS2). Each point represents the average value for three replicate of each variable per sampling date. All data were normalized before performing MDS analysis.

Stress=0.145
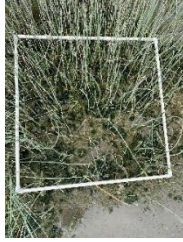
ANOSIM R statistic: 0.1026, significance=0.001

12. Appendix G: Project Budget

Award	Item	Cost
Western Washington University Research and Sponsored Programs Award	1000 12mL Evacuated Glass Exetainers (LabCo)	$506.32
	Methane Gas Standard (Sigma-Aldrich)	$270.12
	Fieldwork Travel	$514.56
	TOTAL	$1,291.00
Western Washington University Huxley Small Grant	Miniature gas regulator and gas-tight 250μL syringe (Sigma-Aldrich)	$177.66
	Micropacked ShinCarbon GC column (Restek)	$350.88
	Exetainer Shipping (LabCo)	$266.62
	Fieldwork Travel	$92.96
	TOTAL	$888.12
Western Washington University Marine and Coastal Science Summer Funding Support	Summer 2021 Stipend	$2,000 +health insurance waiver

13. Appendix H: Vegetation Composition Summary

Table 11. Vegetation Composition at RS1, RS2, RM1, and RM2 throughout project

Date	RS1	RS2	RM1	RM2
August 2020				
October 2020				
February 2021				
May 2021				
June 2021				
July 2021				

August
2021